

# *LYSO experiment*

Alberto Appoloni, Massimo Fellin, Andrea Pegoretti, Nicolò Russo, Erika Socal



# Contents

<b>1</b>	<b>Introduction</b>	<b>5</b>
1.1	Experimental setup . . . . .	5
1.2	Description of the configuration . . . . .	7
<b>2</b>	<b>Data analysis and discussion</b>	<b>9</b>
2.1	Preliminary steps . . . . .	9
2.1.1	Data rejection . . . . .	9
2.2	Results . . . . .	11
2.2.1	Parameter to determine the energy . . . . .	11
2.2.2	Calibration . . . . .	13
2.3	Application of the calibration to cobalt source . . . . .	24
2.3.1	Co-SS . . . . .	24
2.3.2	Co-S-LYSO . . . . .	28
2.4	Am-LYSO-CZT . . . . .	29
2.4.1	Calibration . . . . .	30
2.4.2	Data rejection . . . . .	31
2.4.3	Results . . . . .	33
<b>3</b>	<b>Conclusion</b>	<b>37</b>



# Chapter 1

## Introduction

This experiment involves coincidence measurements from different type of detectors using an oscilloscope, in order to evaluate the energy spectrum of some common sources. To achieve this purpose, calibration of detectors is necessary.

### 1.1 Experimental setup

The detectors used throughout this experiment are: three different NaI(Tl) and a LYSO inorganic scintillators and a CZT solid state detector.

The NaI(Tl) was widely described in the first report. As written there, its main property is the large light yield when excited compared to other inorganic scintillators.

On the other hand, the LYSO is characterized by a lower decay time response  $\tau = 40\text{ns}$ , allowing for higher time resolution. The problem with this device is its intrinsic background due to the radioactive decay of the isotope Lutetium-176, present in 2.6% in the bulk of the detector, which has a mean half-life time of about  $T_{1/2} = 38\text{Gy}$ .

This chemical specie undergoes a  $\beta^-$  decay with two different branching ratio. Since the electrons emitted have low energies, the range of the propagation in the material is small and the re-absorption takes place. For example an electron with energy  $E = 596\text{keV}$  (the maximum produced in this process) will travel in the LYSO for fractions of millimeter (considering the material density as  $\rho = 7.1\text{g/cm}^3$ ).

Furthermore, after the  $\beta^-$  decay the nuclei are left in an excited state and go back to the ground state via  $\gamma/X$ -emission. In a general case, it is known that photons can interact with matter via three different processes, whose probability of occurrence depends on their energy: photoelectric effect, Compton scattering and pair production. Photons in this particular process have an energy equal to  $E = 88\text{keV}$  so the dominant contribution is the photoelectric effect, for which it is totally absorbed by the atom and it contributes to the intrinsic background.

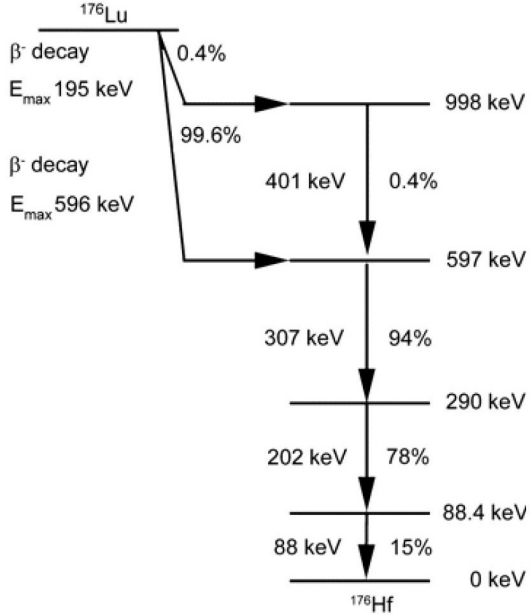


Figure 1.1: Decay chain of the Lutetium-176.

Both NaI(Tl) and LYSO need a PMT to convert the scintillating light into an electrical signal. The PMTs are alimented at 1100V by means of an high voltage module to enhance the gain.

The CZT is a cadmium zinc telluride semiconductor belonging to the class of solid state detectors. Compared to a germanium detector, it is characterized by a wider band gap between the conduction and valence band that allows to use it without the need of liquid nitrogen cooling processes, since the thermal energy is not enough to have a dominant background. However, this fact leads to a lower number of information carriers and thus to lower energy resolution. The CZT is alimented with an high voltage supply (900V) to enlarge the depletion region and ensure an inversely polarized junction. Since the signal produced is extremely small, it needs to be amplified using a preamplifier alimented at  $\pm 12\text{V}$ . CZT has an higher energy resolution compared to inorganic scintillators, but it is extremely slow in the collection of the signals, as charges take large time to drift towards the external acquisition apparatus.

The last device adopted is a 40Gsample/s oscilloscope, equipped with 4 input channels and able to implement during the data acquisition 12 analytical functions. The oscilloscope is used in an almost-shortcut configuration ( $50\Omega$ ) to avoid reflection of the signal with the cables coupling. It contains a low-pass-filter with cut frequency that can be set by the user, in this experience the threshold was chosen at  $20\text{MHz}$  since the signal are quite slow. As a consequence, the lost of information cannot be avoided but a smoothed signal is implemented for free. To trigger the acquisition, the pattern options can been selected. The oscilloscope will trigger only when the signal in the input channels will drop below (0 boolean element)

or overcome (1 boolean element) the trigger level. This distinction is necessary because the detectors connected to the oscilloscope produce a signal that can be positive (CZT and second-last diode of the LYSO<sup>1</sup>) or negative (NaI(Tl) and last diode of the LYSO). The LYSO signal arrives at the oscilloscope 100ns in advance compared to NaI(Tl). In order to achieve coincidence, a cable to increase the path of the light is introduced: since light in the BNC cable travels at about 20cm/ns, a 20m long cable is needed.

## 1.2 Description of the configuration

The equipment described so far are employed in the experiment and coupled in different way to determine the energy spectrum with more than one detector. The coincidence configurations used in this experience must be divided depending on the day at which it is performed, as the initial condition for each run are different. In the first laboratory day, the following configurations have been tested:

- a *Triple* containing two NaI(Tl), one in front of the other, in coincidence with the anode output of the LYSO, that is placed in the middle to measure the background, without any other source
- a *Na-triple* in which the sodium source is added to the previous setup and the detectors are opportunely rearranged
- a *Na-SS* analyzes the sodium source with the aid of two NaI(Tl) scintillators in coincidence
- the *Co-SS* substitutes the sodium source with a cobalt one
- the *Na-S-LYSO* substitutes one NaI(Tl) in the previous configuration with the LYSO
- a *Co-S-LYSO* replace the sodium source with the cobalt
- the *S-LYSO* takes the background

Several weeks after this data taking, a new configuration has been implemented, namely the *Am-LYSO-CZT*, where the two detectors have been placed between an americium-241 source. The calibration of the setup has been performed with sodium and cobalt, but the short acquisition time leads to not sufficiently large set of data that limits the validity of the statistics.

---

<sup>1</sup>The signal on this diode is positive and is used when the anode saturate, since it contains a lower amplified signal.



# Chapter 2

## Data analysis and discussion

### 2.1 Preliminary steps

#### 2.1.1 Data rejection

Among the whole data set, some event must be rejected as they do not represent reliable physical results.

##### Saturation

The first cut is the saturation of the signal in the oscilloscope. This phenomenon is evaluated, as already explained in the previous report, looking at the proportionality between the mean (or the area, i.e. the parameter that represents the energy of the event) of the signal with respect to the peak-to-peak amplitude. Figure 2.1 shows this phenomenon: in the right part of the graph some points that have constant peak-to-peak distance but different mean value.

##### Baseline

The second cut concerns the baseline of the signals. Plotting in a single graph the baseline registered for the whole dataset, the good data which should be taken are those contained within  $3\sigma$  from the central value of the Gaussian distribution. Figure 2.2 is an example and the rejected event are those outside the bell-shaped curve.

##### Triggering time

A similar request is done for the difference between the time at which each channel of the oscilloscope is triggered (see Figure 2.3 for an example): too far or too close time trigger are suspicious and the event must be rejected.

Additionally, an anomalous behaviour can be seen in the high peak at 0 time delay. These events can be explained by the fact that the trigger window chosen for the experience was

insufficient to account correctly for them, i.e. the triggering time was before or after the chosen band in the oscilloscope.

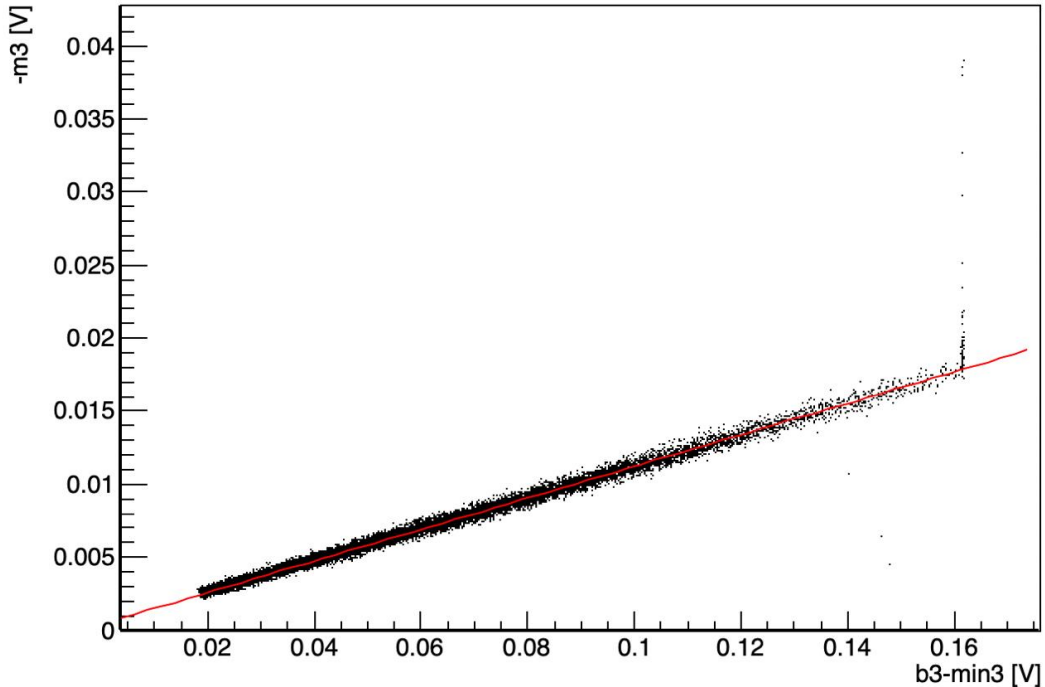


Figure 2.1: Example of signal saturation for the *Triple* configuration, considering the distance between the minimum and the baseline ( $x$  axis) and the mean ( $y$  axis).

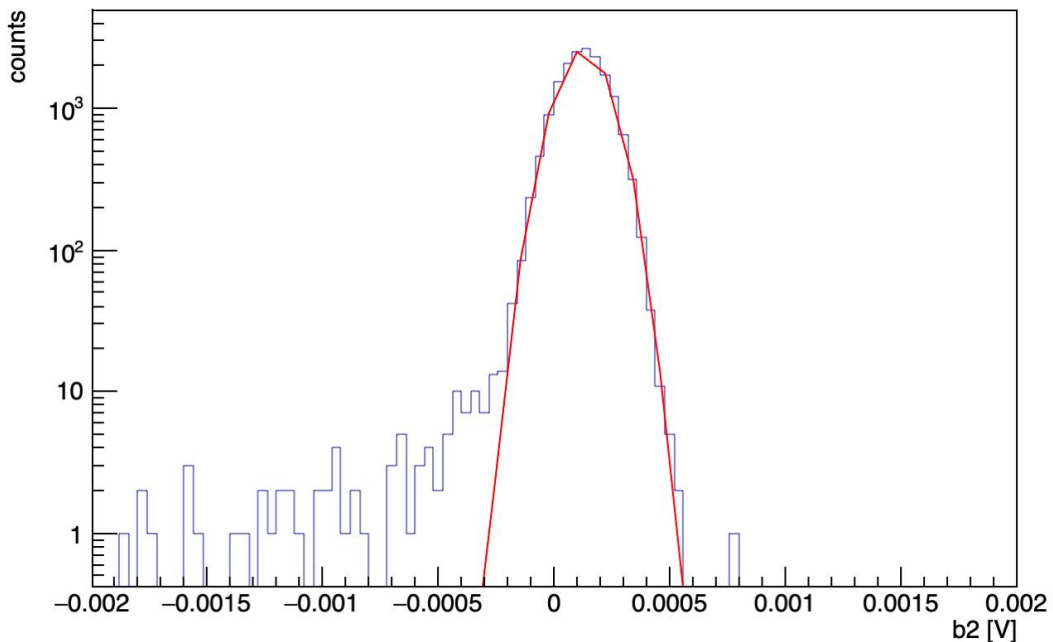


Figure 2.2: Baseline *veto* for the *Triple* configuration.

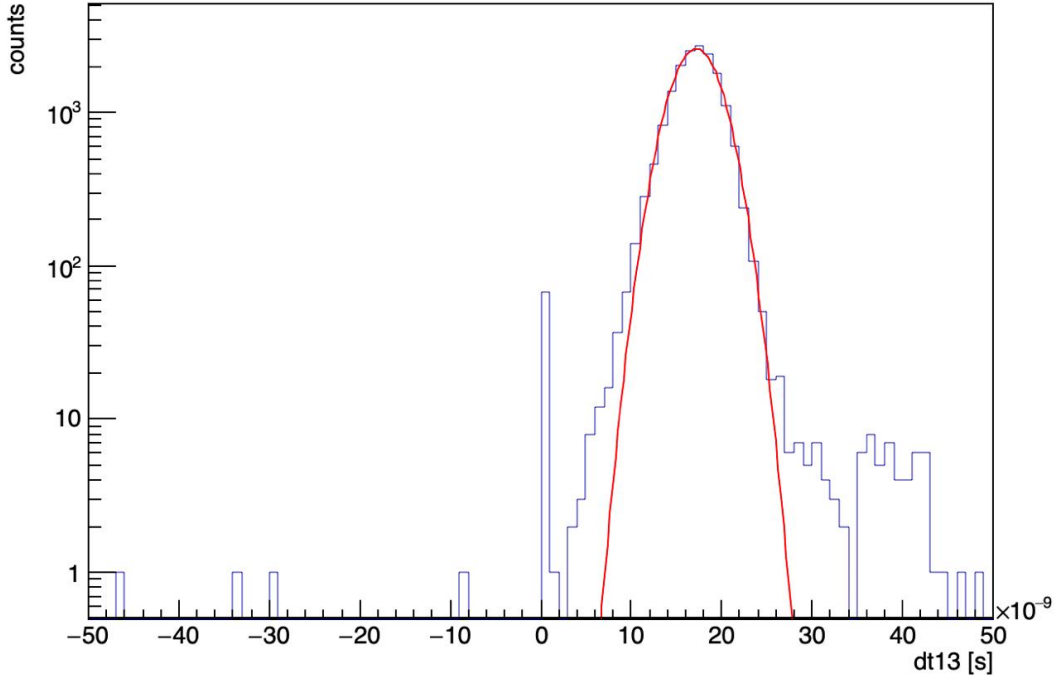


Figure 2.3: Time difference between triggers of scintillator and LYSO in the *Triple* configuration.

## 2.2 Results

### 2.2.1 Parameter to determine the energy

The oscilloscope has some functions that can be implemented during the data taking, that allow to estimate the energy of each event in different ways to better determine the parameter which is more precise. These parameters are the area of the signal, evaluated from the baseline to the deepest peak, the mean value and its median. The procedure of determination of the best parameter is applied for only one of the previously listed configuration, namely the *Na-triple*, assuming that the discussion will be valid for all the other setups. The parameter that better describes the energy is the one with the smallest full width at half maximum (FWHM) in the Gaussian distribution fitting the peaks, that allows to have higher precision and resolution in the measurement.

After the data acquisition, the 2D histogram plotting their value vs the number of counts is done and the three peaks expected for the Na-22 decay are fitted with the Gaussian. These are: one from the de-excitation of the neon at  $E = 1.274\text{MeV}$ , another peak at  $E = 511\text{keV}$  relative to one of the two photons coming from the annihilation of the positron (as they are emitted back-to-back and only one can strike the detector) and the most energetic one that results from the pile-up process, i.e. the sum of the previous two that arrives at the same time and are seen as a single event.

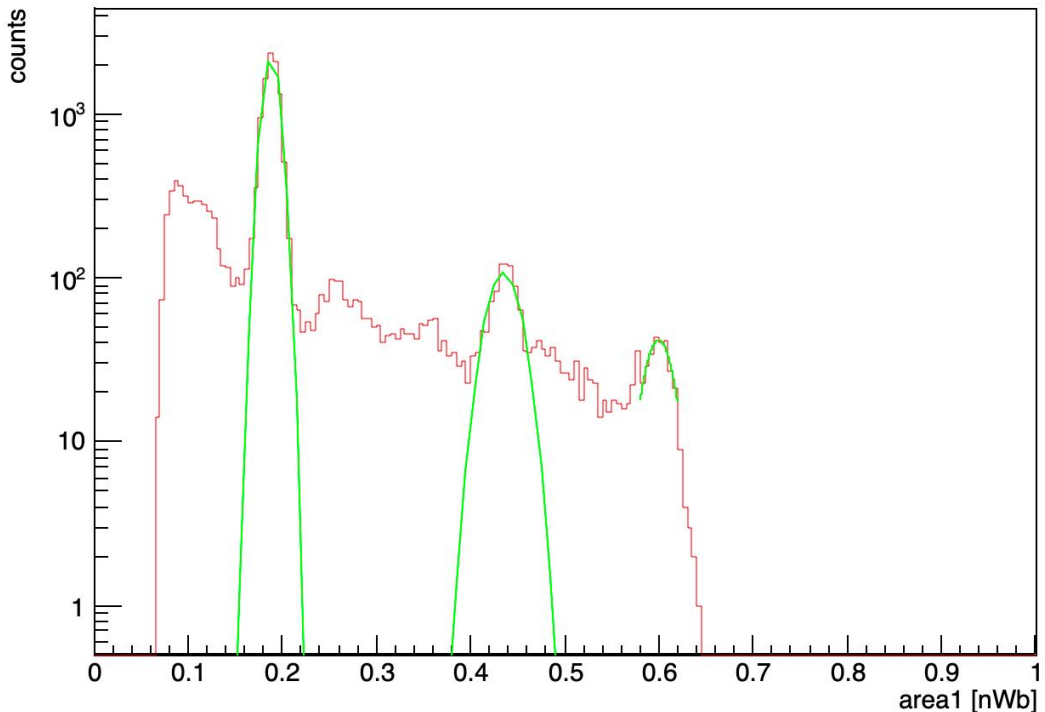


Figure 2.4: Energy peaks evaluated as the area of the signal reported in the oscilloscope for the *Na-triple* configuration.

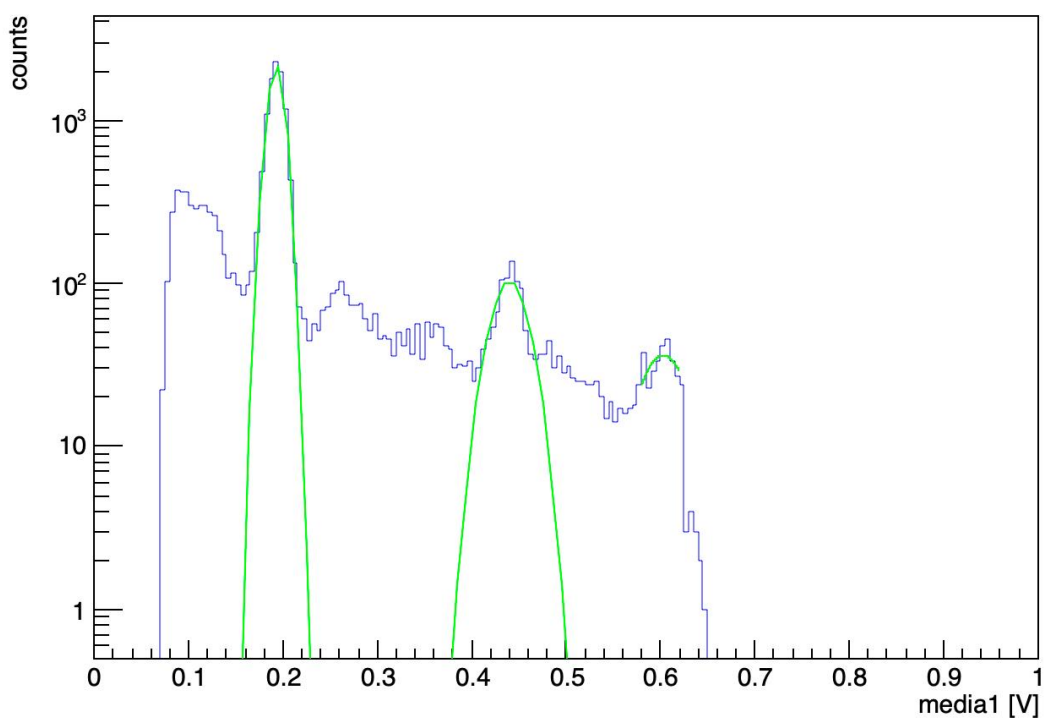


Figure 2.5: Energy peaks evaluated as the mean of the signal reported in the oscilloscope for the *Na-triple* configuration.

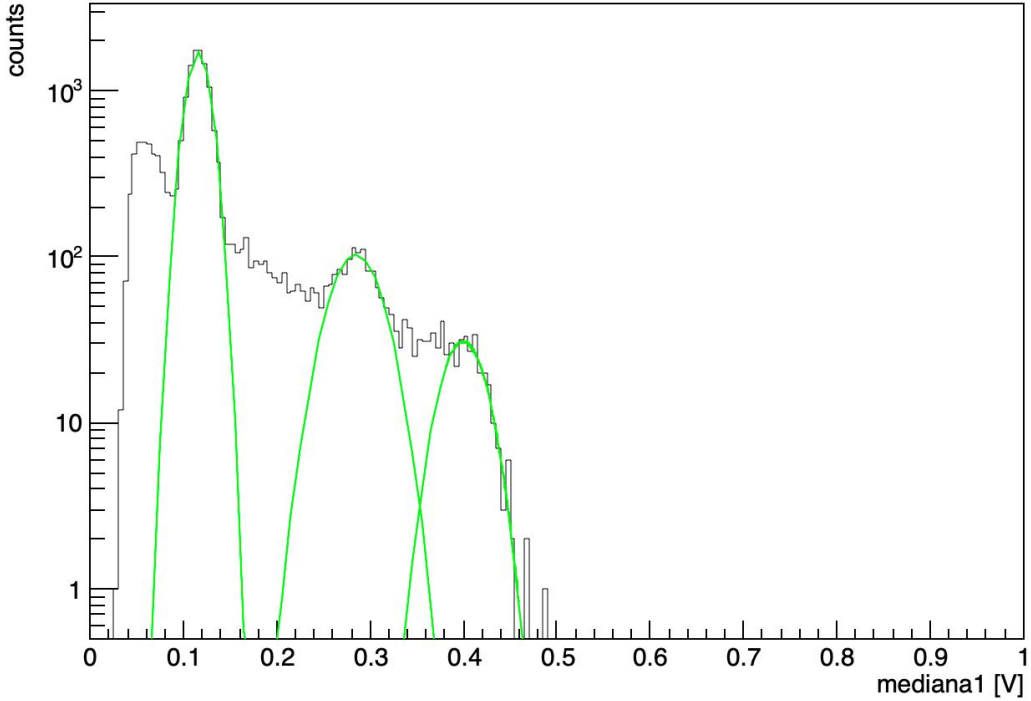


Figure 2.6: Energy peaks evaluated as the median of the signal reported in the oscilloscope for the *Na-triple* configuration.

	area	mean	median
peak 1	$0.0201 \pm 0.0001$	$0.0207 \pm 0.0002$	$0.0291 \pm 0.0004$
peak 2	$0.040 \pm 0.002$	$0.044 \pm 0.002$	$0.061 \pm 0.005$
peak 3	$0.036 \pm 0.005$	$0.038 \pm 0.002$	$0.052 \pm 0.005$

Table 2.1: FWHM estimation for all the peak given by the Gaussian fit.

Figures 2.4, 2.5 and 2.6 summarize the result described so far. For each of the three graphs, the  $y$  axis is expressed in logarithmic scale to better appreciate the presence of the peaks. Tables 2.1 summarized the FWHM and the relative error for the three peaks in the three cases. This Table clearly shows that the best parameter is the area. However, since this analysis was done after the whole data taking, during the acquisition in the laboratory the mean was chosen as estimator for the energy.

### 2.2.2 Calibration

The following step is the calibration of the detectors. This step is fundamental and must be done before every data acquisition, as its aim is to determine the energy-mean conversion. To calibrate the LYSO, the sodium source is used, as its decay peaks are well known, while

for the calibration of the scintillators, both the sodium and the intrinsic radioactivity of the LYSO are used. The results of this step is shown in Figures 2.7, 2.8, 2.9 and 2.10.

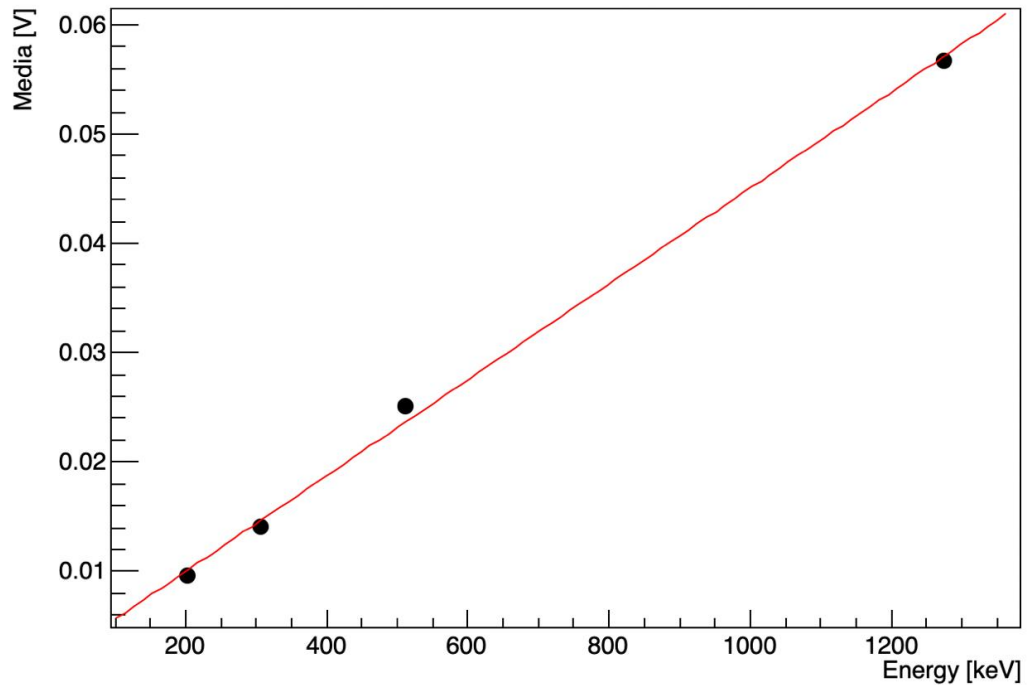


Figure 2.7: Calibration curve of the first scintillator.

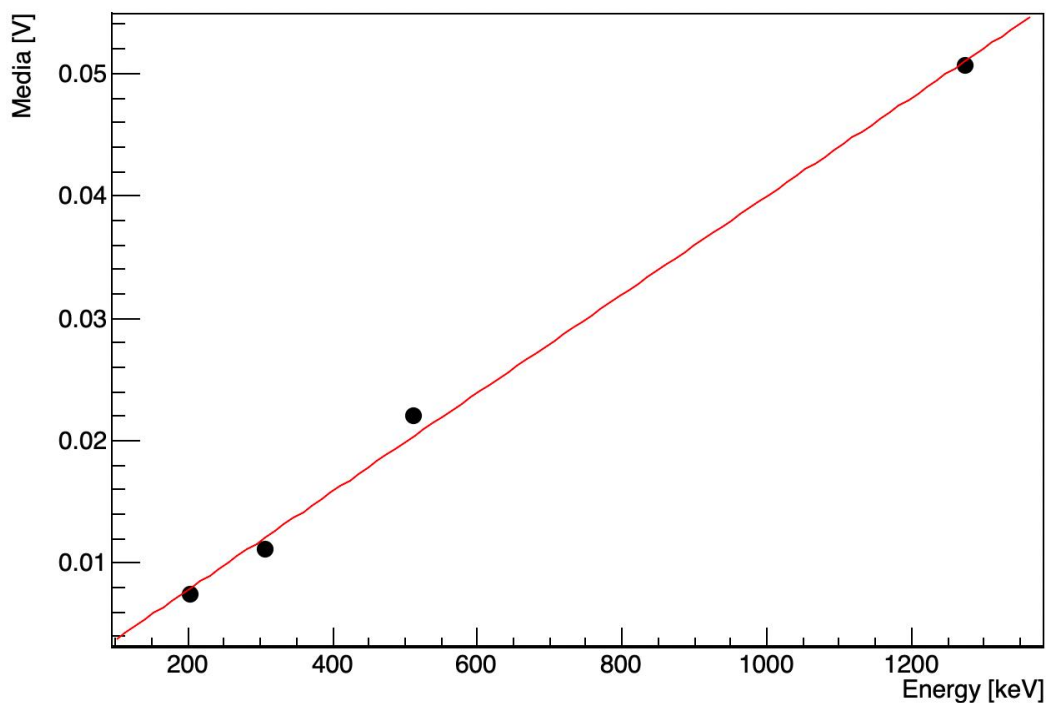


Figure 2.8: Calibration curve of the second scintillator.

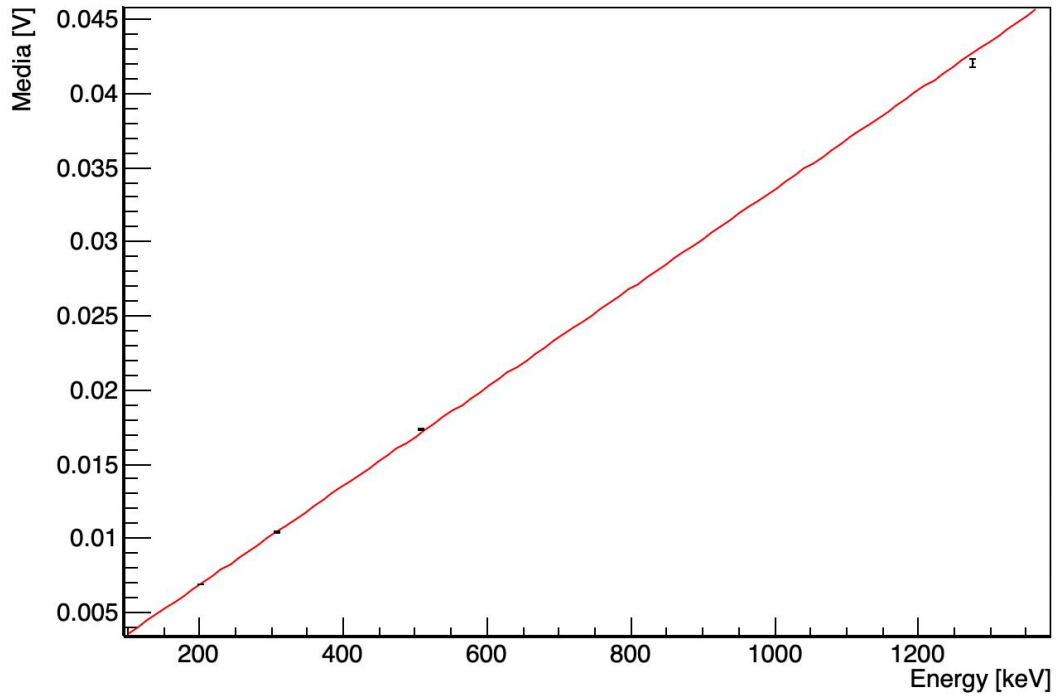


Figure 2.9: Calibration curve of the third scintillator.

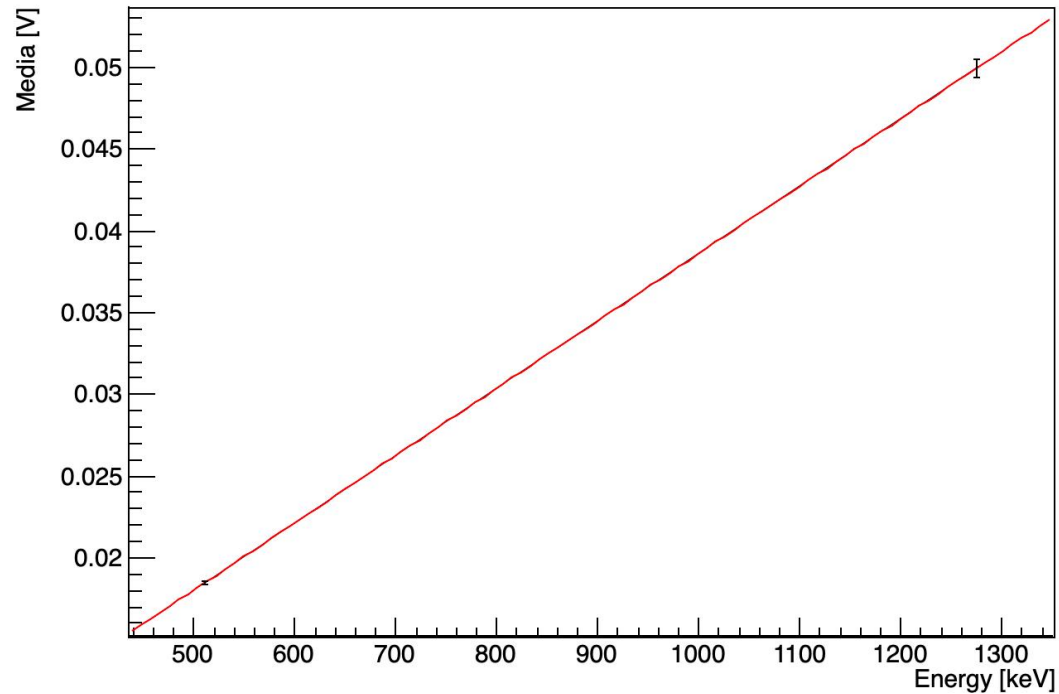


Figure 2.10: Calibration curve of the LYSO.

A relation that is interesting to check is the behaviour of the energy resolution of the peaks, evaluated as the  $\sigma$  in the Gaussian fit with the energies, assuming an exponential background, since often these peaks lie on the Compton shoulder of other peaks. The expected behaviour

is explained in Equation 2.1:

$$\sigma = \sqrt{p_0^2 + (p_1 \sqrt{E})^2} \quad (2.1)$$

where  $p_0$  belongs to baseline fluctuations related to electronic noise and  $p_1$  represents the Poissonian statistical fluctuations. Here, only 2 d.o.f. are present, hence the plot has very few points and the fit parameters are determined approximately and do not faithfully reproduce the trend.

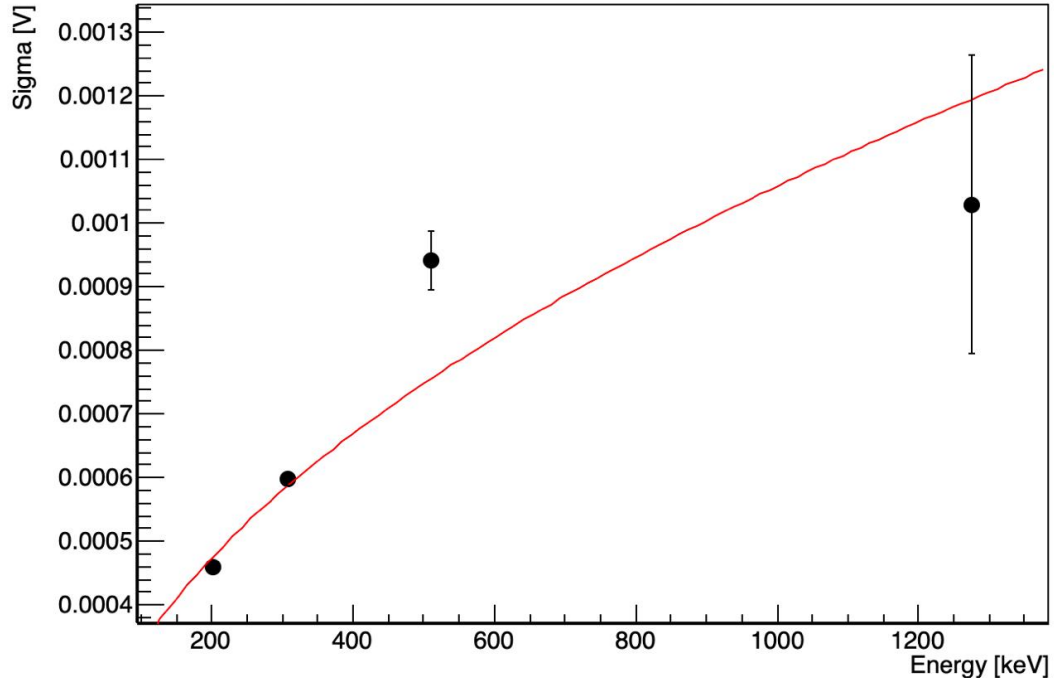


Figure 2.11: Behaviour of the energy resolution with the increasing energies of the peaks in the calibration process.

The following subsections show the results obtained during the calibration procedure using the sodium source, and additionally the background acquisition without any source.

### Triple

In the *Triple* configuration, two scintillators are placed in coincidence and use LYSO as radioactive source.

Figure 2.12 is a 2D histogram that shows on the  $x$  axis and on the  $y$  axis the energies of the first and second scintillator respectively, after the proper calibration. Two main trends are clearly visible: when scintillator 1 measures one photon with specific energy (either  $E = 202\text{keV}$  or  $E = 307\text{keV}$ ) the other scintillator detects the other photon, and *vice versa*. A third zone of concentration of signal is present in the diagonals  $E_1 + E_2 = 202\text{keV}$  and  $E_1 + E_2 = 307\text{keV}$ , belonging to the Compton effect for which a (back)scattered photon can be seen from both the scintillators. A note to be done is the absence of the signal for

photons at  $E = 88\text{keV}$ , which is the dominant emission by lutetium. The reason relies in the complete absorption by the LYSO matter of this radiation due to its low energy.

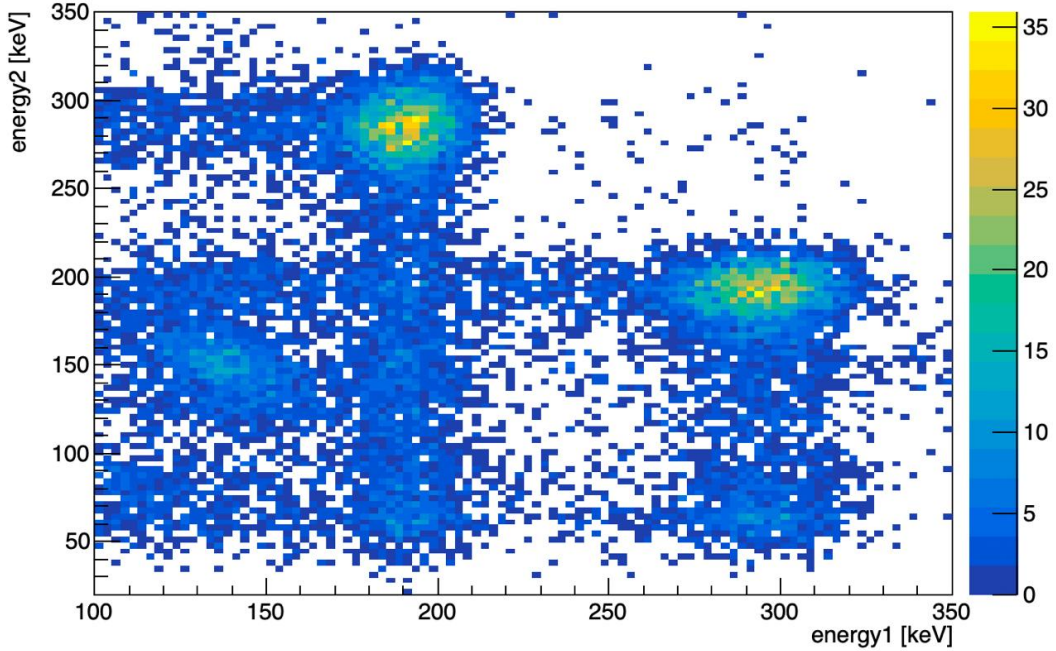


Figure 2.12: Plot of the event seen by the two scintillators in coincidence. The two decay products of the lutetium and a Compton trace are visible.

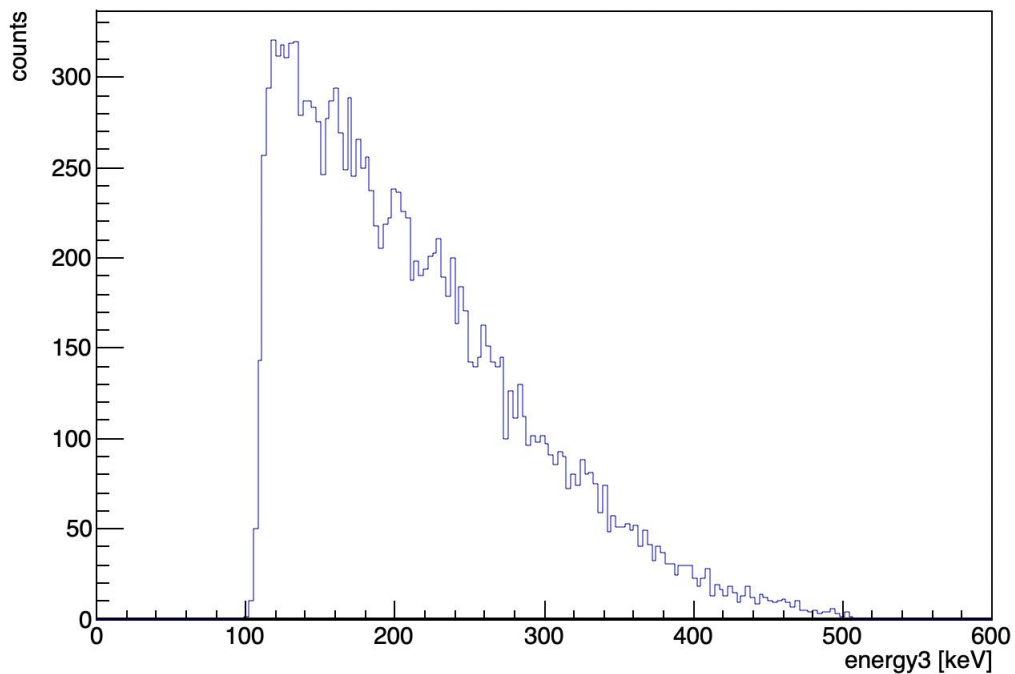


Figure 2.13: Spectrum of the LYSO of its own background. It is interesting to experimentally see that the maximum energy of the intrinsic background is at about the maximum value of the theoretical energy of the electron emission in its  $\beta$  decay.

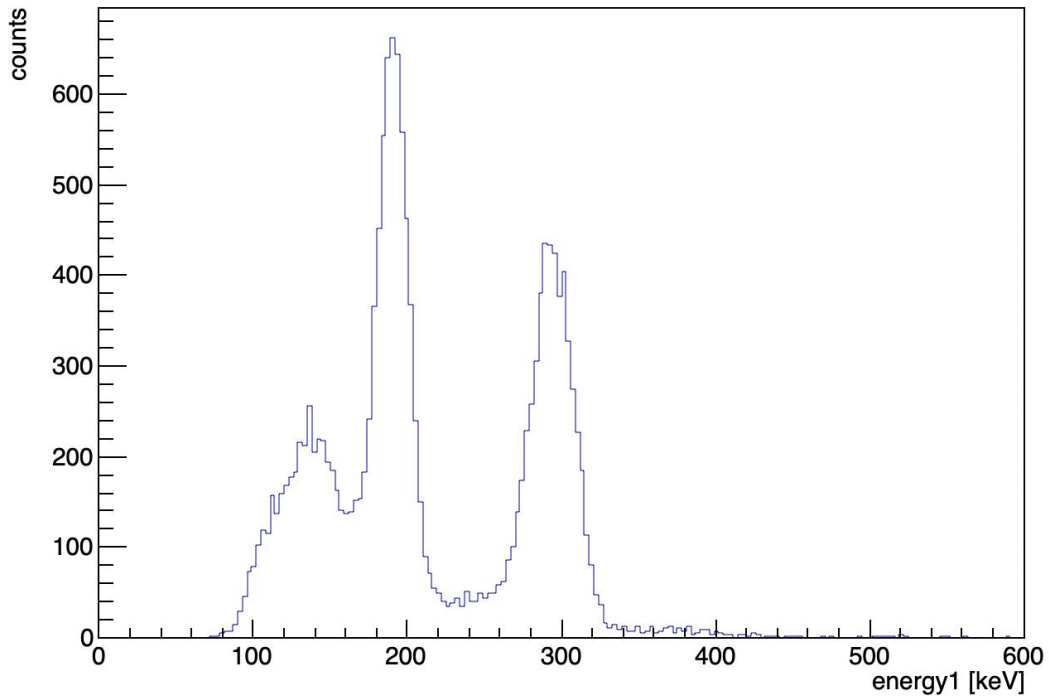


Figure 2.14: Scintillator spectrum. The two peak related to  $E = 202\text{keV}$  and  $E = 307\text{keV}$  are visible, with the Compton shoulder of the  $E = 202\text{keV}$  photon. Probably the Compton shoulder of the  $E = 307\text{keV}$  is covered by the  $E = 202\text{keV}$  peak. The  $E = 88\text{keV}$  peak is not present due to a probable re-absorption.

### Na-triple

The sodium decay channel is schematized in the Figure 2.15.

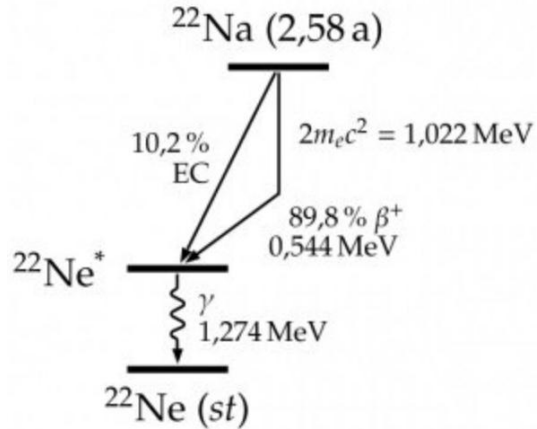


Figure 2.15: Decay chain of the sodium-22 source. The positron emitted in the  $\beta^+$  decay is converted into two back-to-back photons after the annihilation with an electron of the medium.

This analysis is affected by low statistics: after data rejection, approximately 1500 events are taken so the data analysis is not able to highlight all the expected patterns.

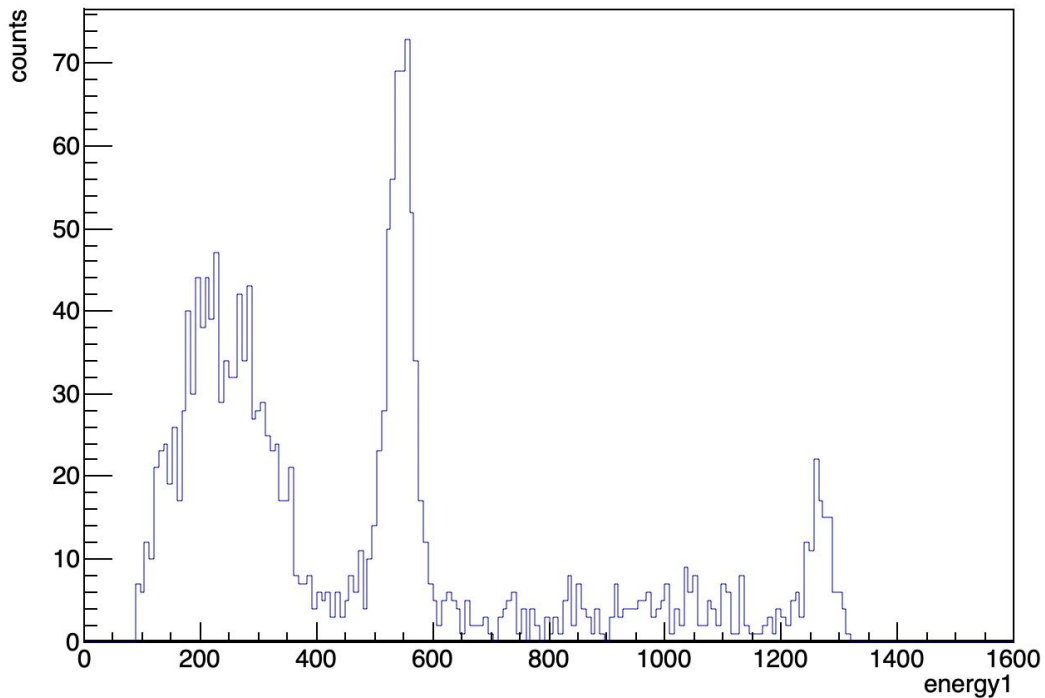


Figure 2.16: Histogram of the counts per energy for one of the two scintillators. A superposition between the LYSO emission spectrum (first peak) and the sodium (last two peaks) can be recognise. LYSO are less shaped because also the Compton shoulder is present.

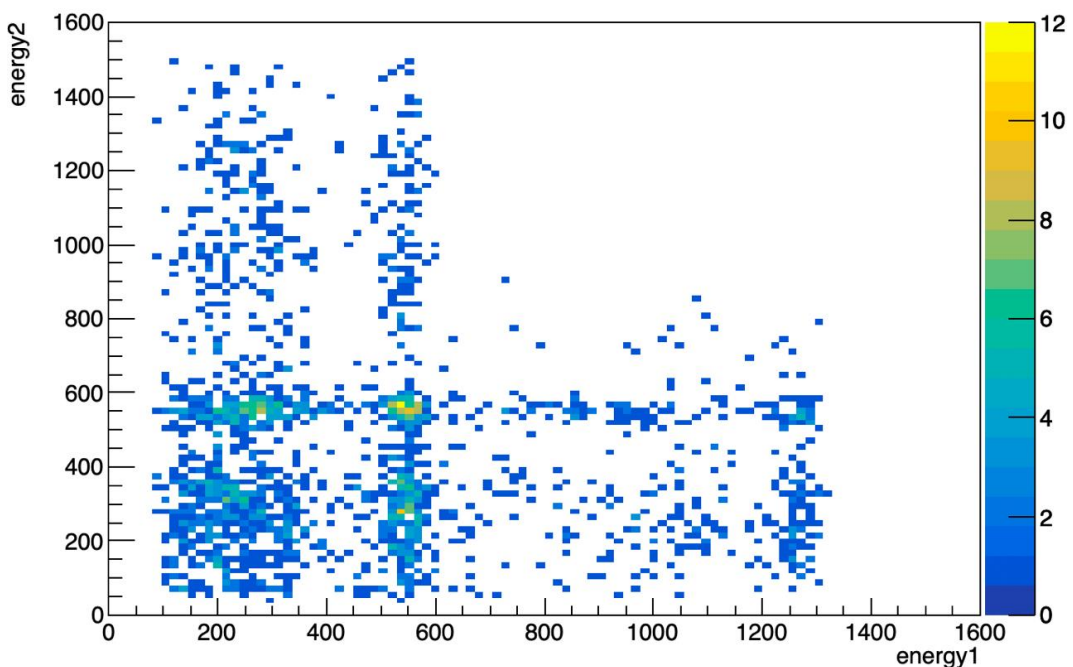


Figure 2.17: Coincidence between the two scintillators. The Compton effect is again visible in the diagonal patterns.

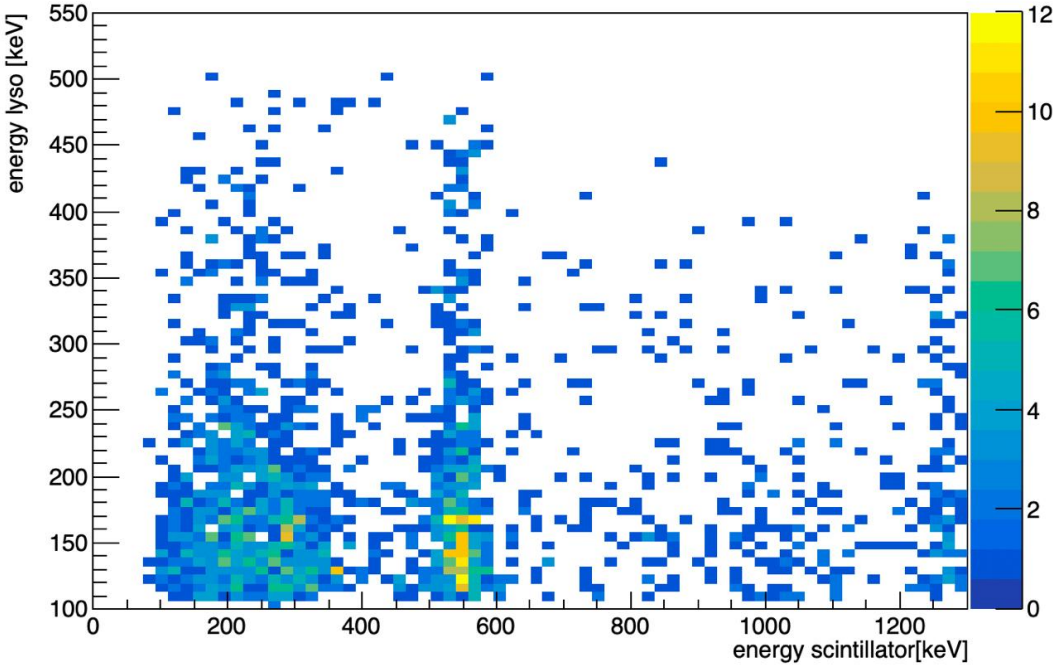


Figure 2.18: Coincidence between LYSO and one of the two scintillators. Unfortunately the poor statistics cannot show the expected 511keV in LYSO dector.

### Na-SS

Figure 2.19 shows the coincidence of the signals between the two scintillators employed in this configuration. The majority of the events are concentrated in the yellow circle that represent the simultaneously detection by the two devices of the two back-to-back photons emitted after the positron annihilation. Again, the diagonal  $E_1 + E_2 = 551\text{keV}$  representing the Compton back scattering is visible.

To better understand the two cross pattern at  $E = 511\text{keV}$  for both the  $x$  and  $y$  axis, Figure 2.20 shows what the scintillator 1 sees when scintillator 2 detects one  $E = 511\text{keV}$ . Basically, what happens is that scintillator 1 gets mostly  $E = 511\text{keV}$  but also its Compton back-scattering, additionally another photons at  $E = 1275\text{keV}$  is seen by the instrument. At around  $E = 1800\text{keV}$  the pile-up peak is visible.

Figure 2.21 shows the similar process for exchanged scintillators. In this case the energy resolution is worst and the identification of the peaks is less evident.

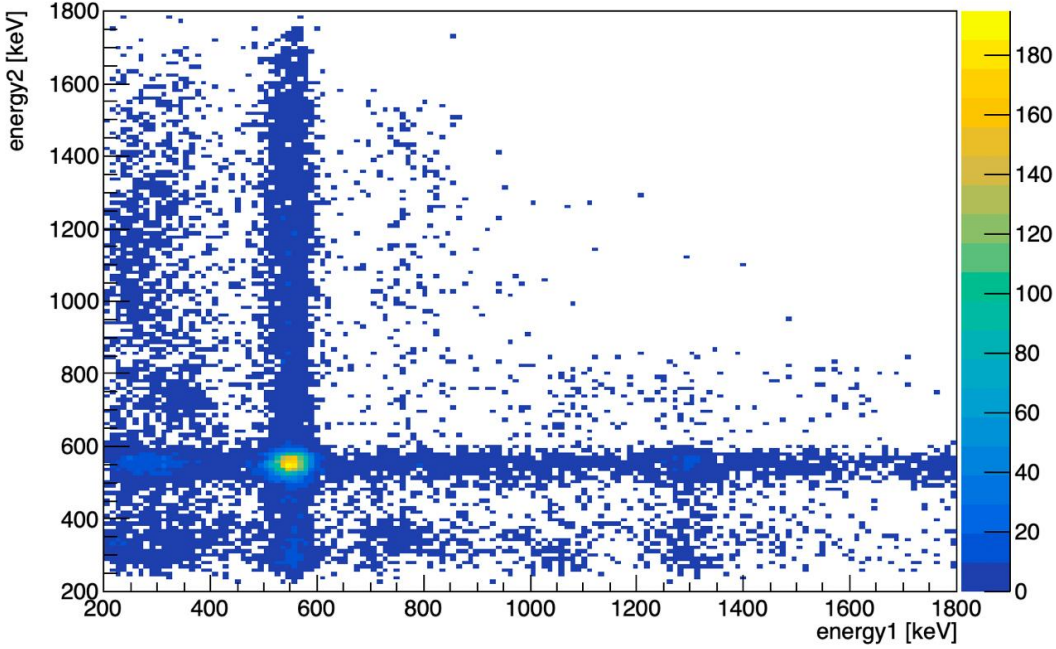


Figure 2.19: Spectrum of the paired scintillators with the sodium source. More data are taken and the pattern of energy distribution is much more visible.

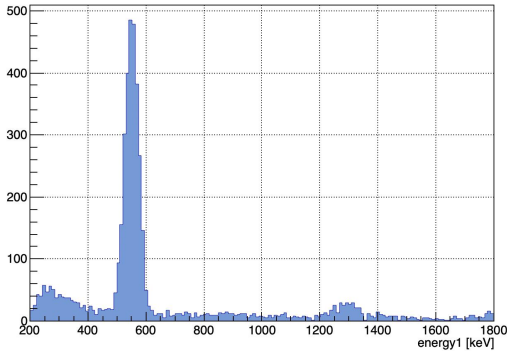


Figure 2.20: Projection of the events seen by scintillator 1 when the energy recorded by scintillator 2 is fixed at  $E = 511\text{keV}$ .

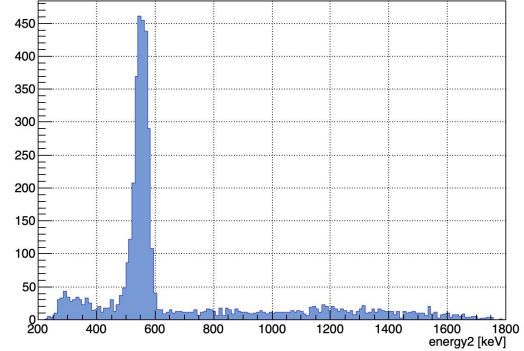


Figure 2.21: Projection of the events seen by scintillator 2 when the energy recorded by scintillator 1 is fixed at  $E = 511\text{keV}$ .

### Na-S-LYSO

A similar analysis is done for the *Na-S-LYSO* configuration.

The enough statistics allows to better highlight the pattern of the energy coincidence. In this case most of the events occur when the scintillator measures  $E = 511\text{keV}$ . Correspondingly, the LYSO sees either the other  $E = 511\text{keV}$  or its intrinsic background at  $E = 202\text{keV}$ .

The LYSO radioactivity at  $E = 202\text{keV}$  and  $E = 307\text{keV}$  is also visible from the scintillator.

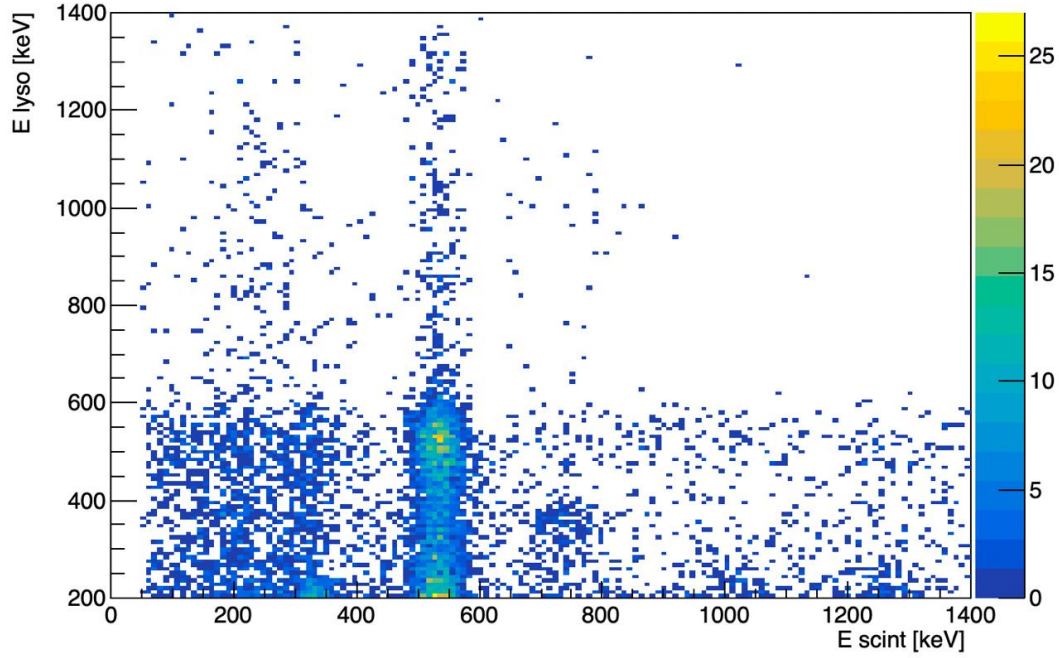


Figure 2.22: Coincidence measurement for the *Na-S-LYSO* configuration. Two dense zone of events are clearly visible when the scintillator records  $E = 511\text{keV}$ , representing either the LYSO radioactivity or the sodium decay.

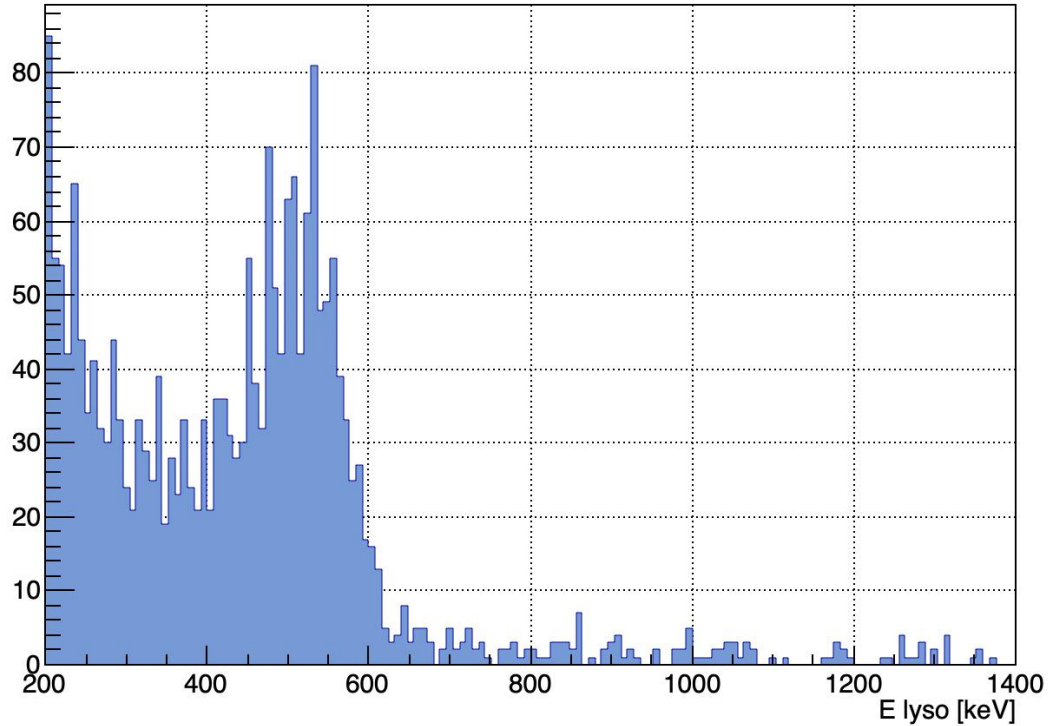


Figure 2.23: Particular view of the LYSO spectrum when the scintillator measures  $E = 511\text{keV}$ .

**S-LYSO**

The events acquired by the *S-LYSO* configuration are basically the intrinsic background of the LYSO detector, as no other sources are present. For this reason, Figure 2.24 is presented, as it reports the scintillator data showing the  $\gamma - X$  emission of the lutetium. The peaks at  $E = 202\text{keV}$  and  $E = 307\text{keV}$  are clearly visible together with their pile-up at higher energies and, as already said, the  $E = 88\text{keV}$  peak cannot be observed due to absorption and the lower energy peak is probably due to the minimum acquisition value of the oscilloscope: indeed, it looks more like an half shaped peak.

The coincidence spectrum in Figure 2.25 describes the same result presented in Figure 2.24, since no other sources are present.

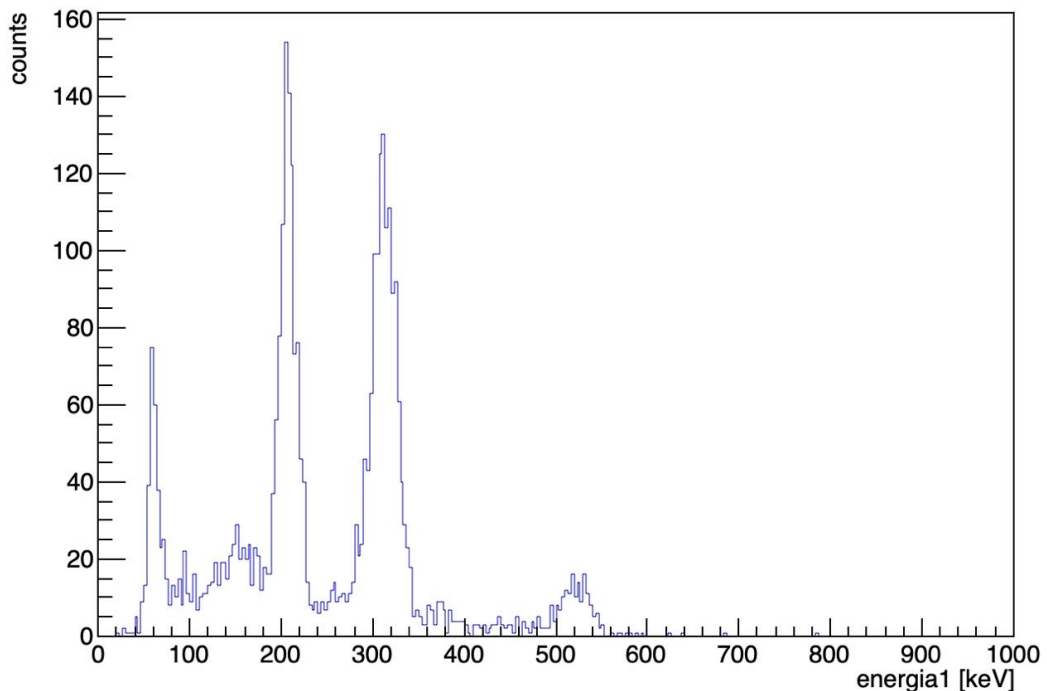


Figure 2.24: Energy spectrum recorded by the scintillator presenting the LYSO intrinsic background relative to the lutetium decay chain.

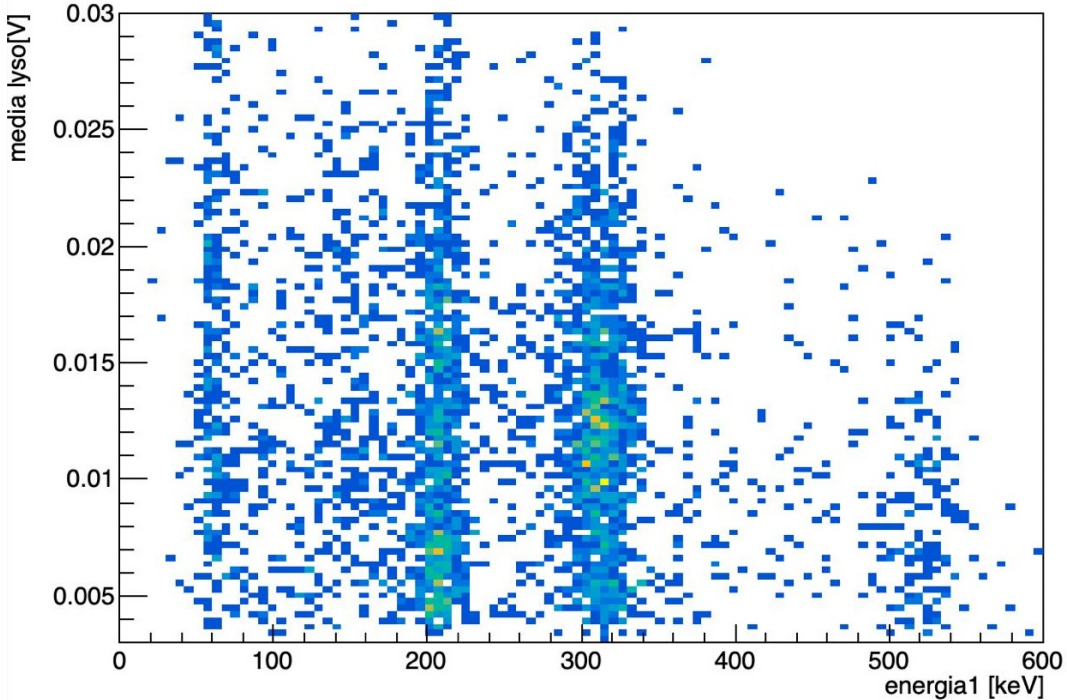


Figure 2.25: Coincidence events seen from both the LYSO and the scintillator.

## 2.3 Application of the calibration to cobalt source

What is done so far can be applied to the determination of the energy peaks of the cobalt source. The decay channel of this element is visible in Figure 2.26:

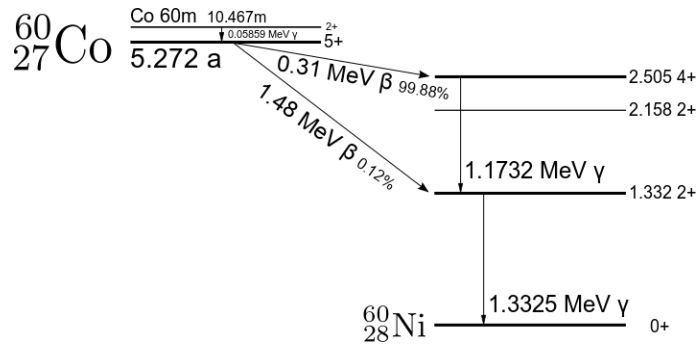


Figure 2.26: Decay of the Co-60.

### 2.3.1 Co-SS

Figure 2.27 is the 2D histogram of the coincidence between the two scintillators. The graph appears anomalous: it presents four circular coincidence pattern rather than the two expected for the cobalt decay in Figure 2.26. This behaviour is even more evident looking at Figure 2.28, in which the most energetic peaks are three rather than two.

To explain this strange behaviour, the energy registered from the scintillator is analyzed as

a function of the number of events, thus with an implicit time dependence. What appear clear from Figure 2.29 is that at certain point the gain of the scintillators increases, inducing modifications on the data acquisition mechanism.

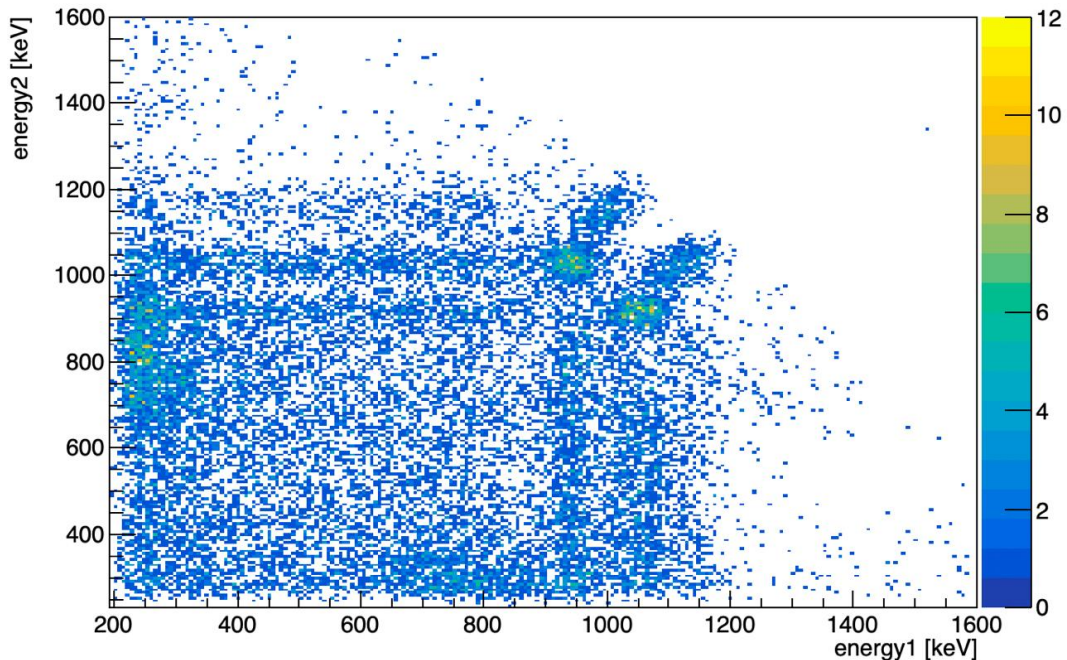


Figure 2.27: 2D histogram of the cobalt decay biased by gain drifting.

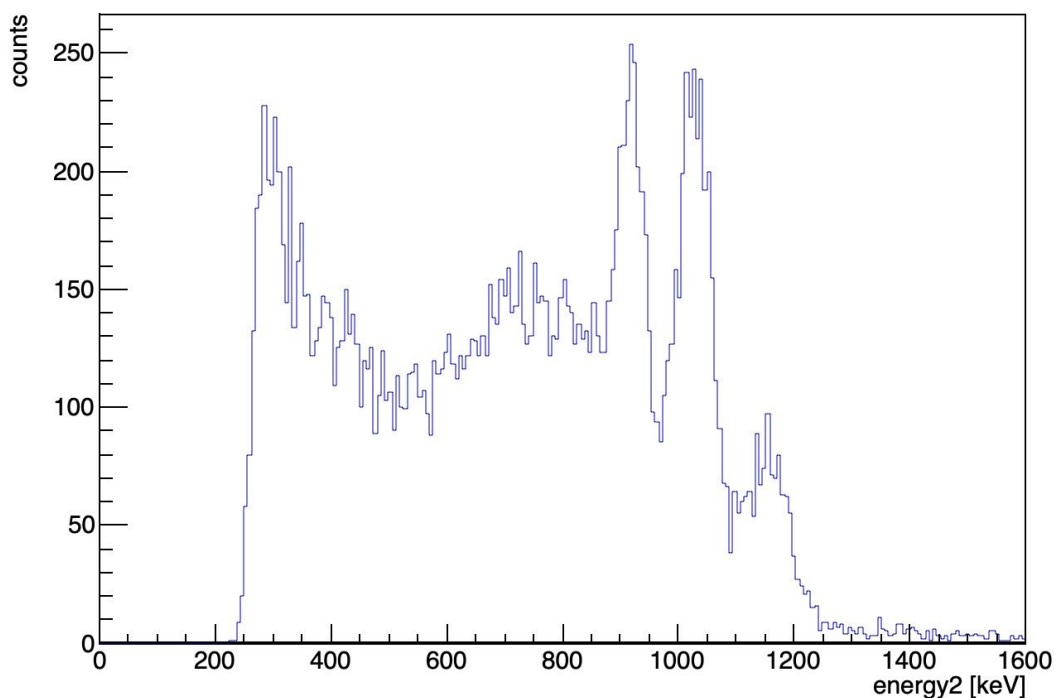


Figure 2.28: Histogram of the counts seen by the scintillator 2 in presence of gain drifting.

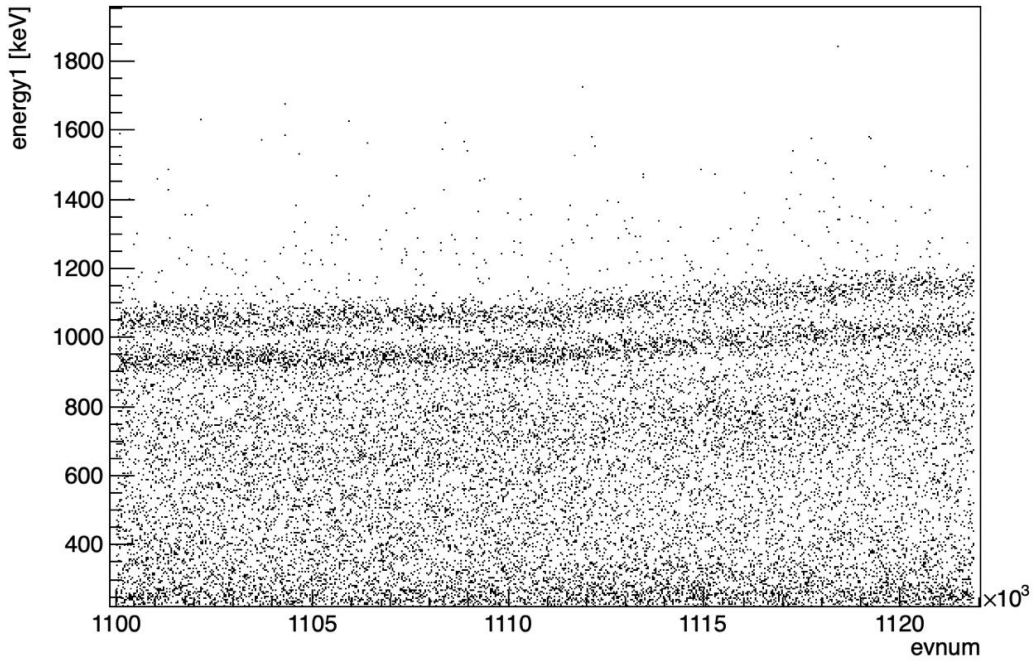


Figure 2.29: Energy as a function of the event number. The drift of the gain is clearly visible in the final part of the pattern, inducing an increasing of the energy registered.

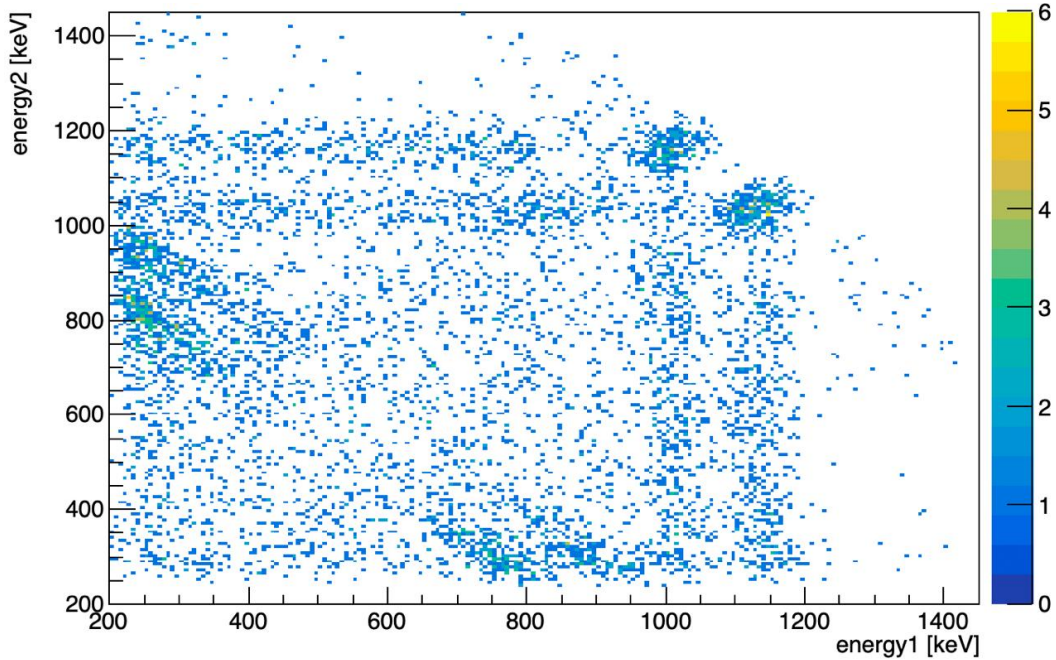


Figure 2.30: Events seen by the two scintillators after data rejection. The Compton diagonal is clearly visible.

Since calibration was performed immediately after these measurements and observing that for the other data takings no gain drifting has occurred, events in Figure 2.29 are cut in order to select only the last points above the transition ending. Figure 2.30 shows the results after this rejection procedure and results in a compatible pattern with the expected one. Despite

this hopeful behaviour, the data rejection significantly reduces the statistics, affecting the reliability of the analysis.

To further analyze the data of this acquisition run, the 2D histograms showing the projections can be plotted. Figure 2.31 is taken looking at scintillator 1 after setting a fixed value of energy  $E = 1300\text{keV}$  in scintillator 2, while Figure 2.32 fixes this energy at  $E = 1100\text{keV}$ . The same can be done fixing the energy on scintillator 1: Figure 2.33 is taken at  $E = 1300\text{keV}$  while Figure 2.34 fixes the energy at  $E = 1100\text{keV}$ . Each one of the main peaks in the four histograms are fitted with a Gaussian distribution using the Likelihood method, since the number of counts are poor, and the program gives the value of energy of the center reported in the captions.

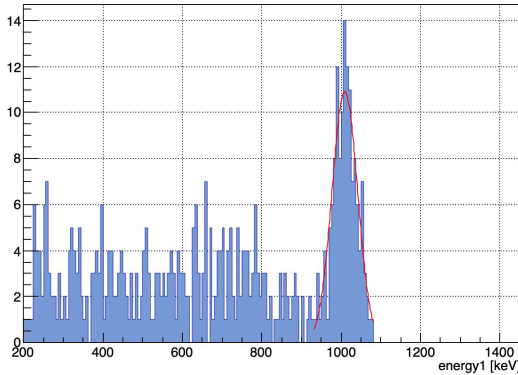


Figure 2.31: Histogram with the Gaussian fit of the peak seen by scintillator 1 when scintillator 2 sees the higher energy photons at  $E = 1300\text{keV}$ . The mean value of the fit is  $E = (1009 \pm 3)\text{keV}$ , non compatible with the expected  $E \simeq 1100\text{keV}$ .

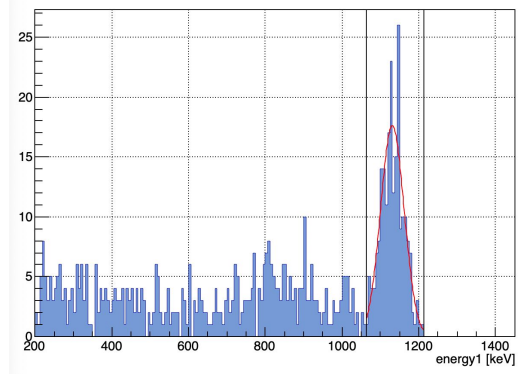


Figure 2.32: Histogram with the Gaussian fit of the peak seen by scintillator 1 when scintillator 2 sees the higher energy photons at  $E = 1100\text{keV}$ . The mean value of the fit is  $E = (1131 \pm 2)\text{keV}$ , non compatible with the expected  $E \simeq 1300\text{keV}$ .

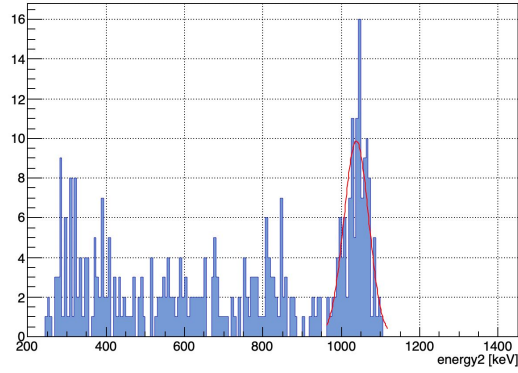


Figure 2.33: Histogram with the Gaussian fit of the peak seen by scintillator 2 when scintillator 1 sees the higher energy photons at  $E \simeq 1300\text{keV}$ . The mean value of the fit is  $E = (1038 \pm 3)\text{keV}$ , non compatible with the expected  $E \simeq 1100\text{keV}$ .

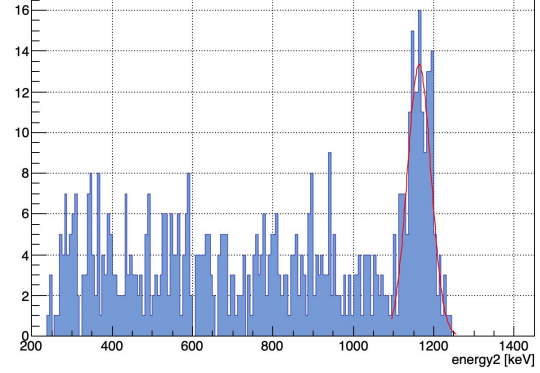


Figure 2.34: Histogram with the Gaussian fit of the peak seen by scintillator 2 when scintillator 1 sees the higher energy photons at  $E \simeq 1100\text{keV}$ . The mean value of the fit is  $E = (1163 \pm 2)\text{keV}$ , non compatible with the expected  $E \simeq 1300\text{keV}$ .

It is evident that each value found by the fit is not compatible with the theoretical expectation. Both of the recovered energies for each scintillator are underestimated, probably

pointing out that the gain of the instruments has not reached the stability and was still changing during the time in between the data acquisition for the cobalt and the calibration with the sodium. At the same time, the fact that each energy is not compatible between scintillators points out that calibration was not good enough, since just four points were considered and larger errors should be associated to energy calibrated. This holds in particular at high energy, where just one point was taken into consideration (1275keV from sodium source).

### 2.3.2 Co-S-LYSO

The cobalt source is also investigate with the LYSO detector. The result obtained in this part of the experience is presented in Figure 2.35.

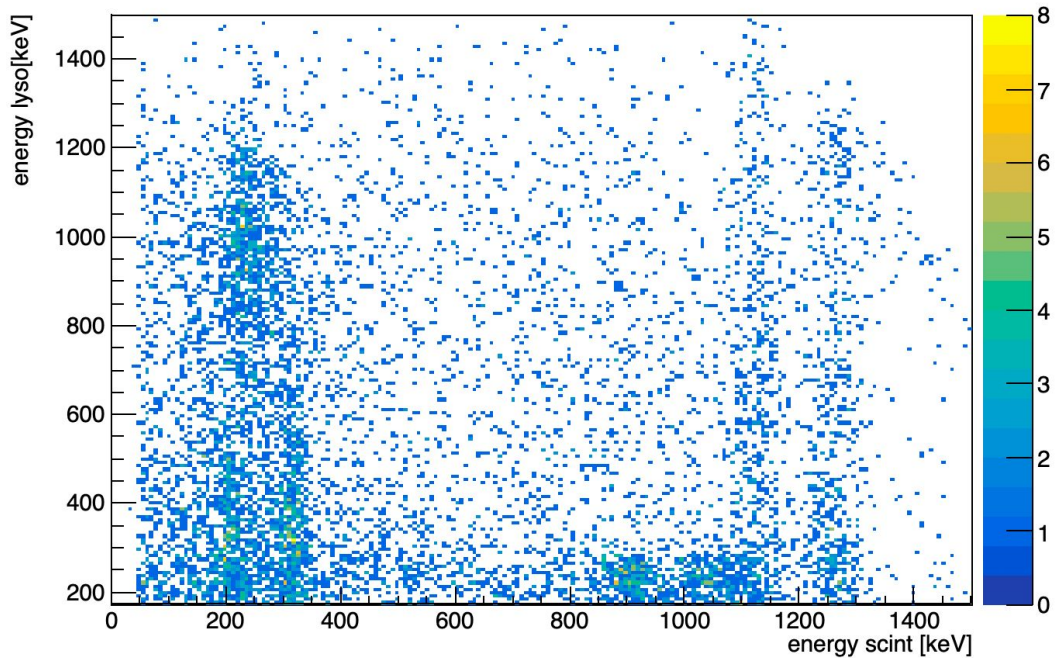


Figure 2.35: Spectrum of the cobalt when the LYSO and the scintillator are present.

Figure 2.35 clearly shows how the scintillator is able to capture distinctly the two cobalt peaks on the right and the LYSO radioactivity on the left. The same cannot be said for the LYSO, for which the Figure highlights the worst resolution of the detector. Despite the large background at low energies, the LYSO sees more dense distribution of events around  $E = 1200\text{keV}$ , while the rest of the graph sees an uniformly distributed pattern. The coincidence seems to be activated most of the time when the scintillator takes the cobalt peaks and the LYSO its own electron background, and *vice versa* when the scintillator registers the photons from LYSO and the LYSO acquires the cobalt peaks.

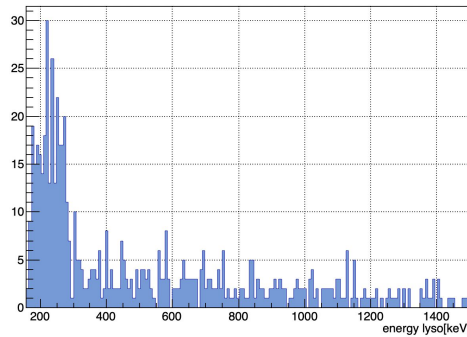


Figure 2.36: Background seen from the LYSO when the scintillator takes the cobalt peaks.

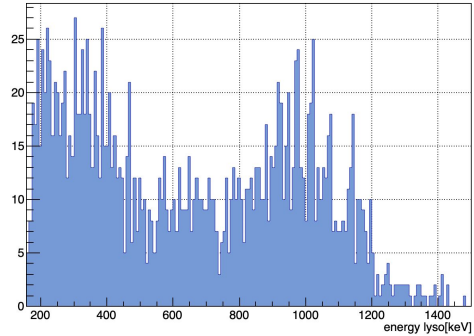


Figure 2.37: Background and cobalt peaks seen from the scintillator when the LYSO takes the cobalt.

Remember that the LYSO has been calibrated using just two peaks, those of sodium source, for this reason, errors on the energy evaluation can be ascribed to imprecision in the calibration because of very low statistics.

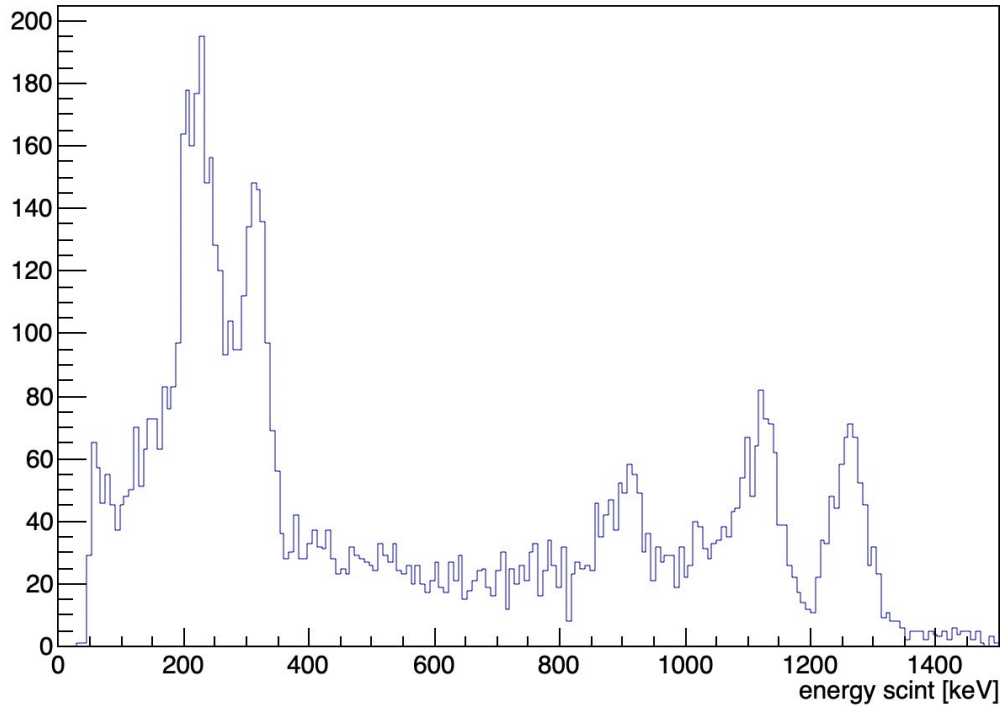


Figure 2.38: Full spectrum of the cobalt (and LYSO) seen by the scintillator. Two Gaussian fit has been performed in the last two peaks, giving as means:  $E_1 = (1115 \pm 2)\text{keV}$  and  $E = (1260 \pm 2)\text{keV}$ .

## 2.4 Am-LYSO-CZT

Figure 2.39 presents the main decay channels, with relative probability, of the americium-241, which is the last radioactive source used this experience. In this experience the measurement of the spectrum of americium-241 is performed in coincidence between LYSO and CZT.

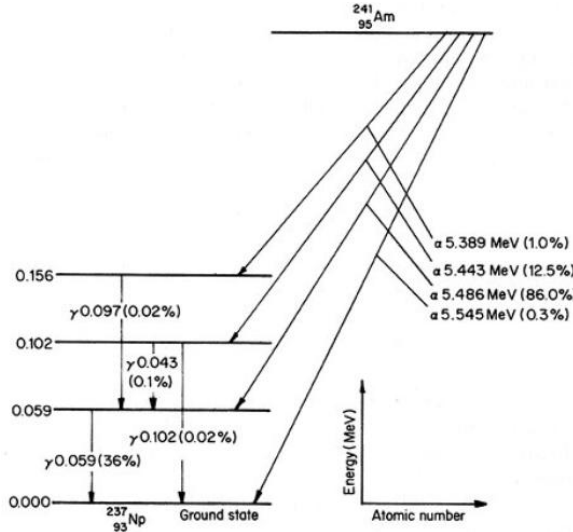


Figure 2.39: Decay channel of americium-241.

All the detectors are extremely sensitive to external light. For this reason they are sufficiently shielded with metallic materials to avoid external noise. The shielding is not able to block  $\gamma - X$  rays so the data acquisition performed so far is not affected, but massive particles like alpha are not able to penetrate and reach the bulk of the detectors. As an example, an alpha particle with energy  $E = 5.486\text{MeV}$  stops in just  $25\mu\text{m}$  of aluminium. For this reason the LYSO uncovering is necessary and the source of americium is placed right in front of its surface. After this modification of the setup, a new covering is needed, so the apparatus was placed inside a paper box fixed with tape, to maximally reduce the light background.

### 2.4.1 Calibration

The first step of this experience is a new run to perform the calibration both for LYSO and CZT. Indeed, a re-calibration of the LYSO is needed even though it was already done, since the measurement took place several days after the first one and parameters, like temperature, can vary day by day affecting the final result.

Again, calibration has been highly unsuccessful since statistic was very poor: CZT has been calibrated exploiting the LYSO  $E = 202\text{keV}$  and  $E = 307\text{keV}$  and the  $E = 511\text{keV}$  of the sodium source, on the other hand it has been impossible to calibrate the LYSO and therefore we will refer to it with the height of the peaks in the oscilloscope and never with the energy, because no mean was extracted. Figure 2.40 reports the three points found for the CZT calibration, where the intercept of the straight line is set to the fixed value 0.

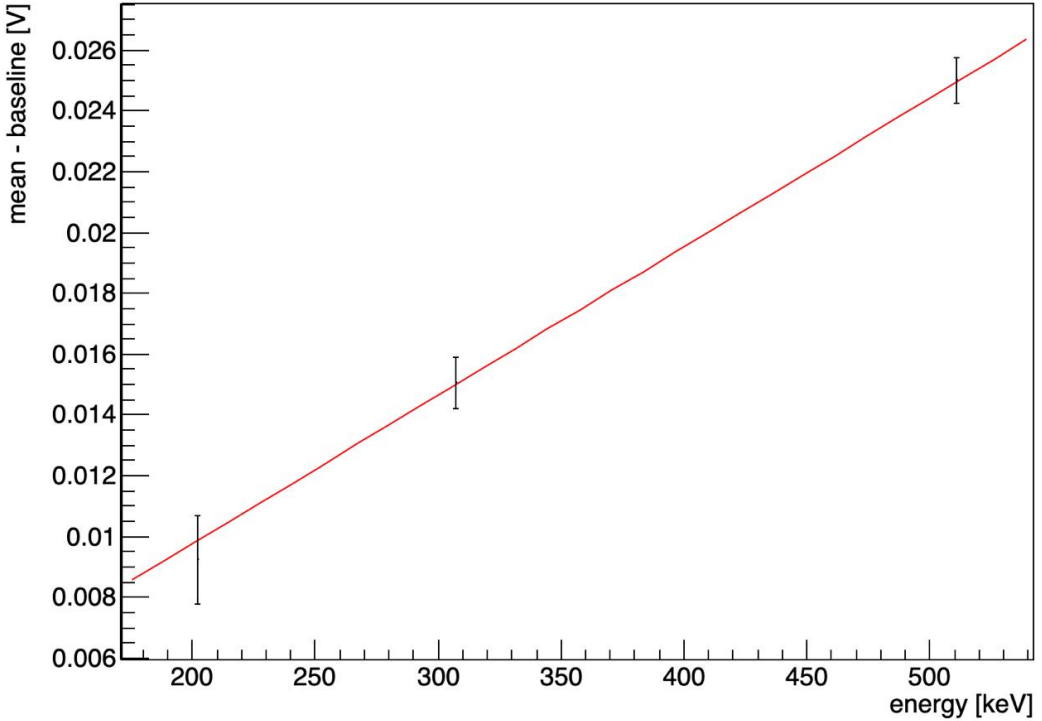


Figure 2.40: Calibration straight line of the CZT detector.

#### 2.4.2 Data rejection

Also in this part of the experience, data rejection is necessary to consider only valuable events, that do not mislead the analysis results.

The first rejection to apply is the coincidence between the signals from LYSO and CZT. As can be seen from Figure 2.41, lots of points are not in coincidence and the time distance registered goes beyond  $10\mu s$ . This value of delay corresponds to a difference of length of BNC cables of  $2km$ , which is clearly unphysical. This problem for sure arises from the oscilloscope, since a fixed band was chosen for the triggering procedure. To clean the data, an arbitrary window in the range  $(0, 5)\mu s$  is chosen, and all the points outside this region are discarded.

A further cut on the trigger time has been implemented and is the one for the LYSO: the excluded values are those placed closed to  $t = 0\mu s$ , since they provide quite unreasonable height of the CZT signal. Figure 2.42 shows the events and the relative time at which the LYSO triggers.

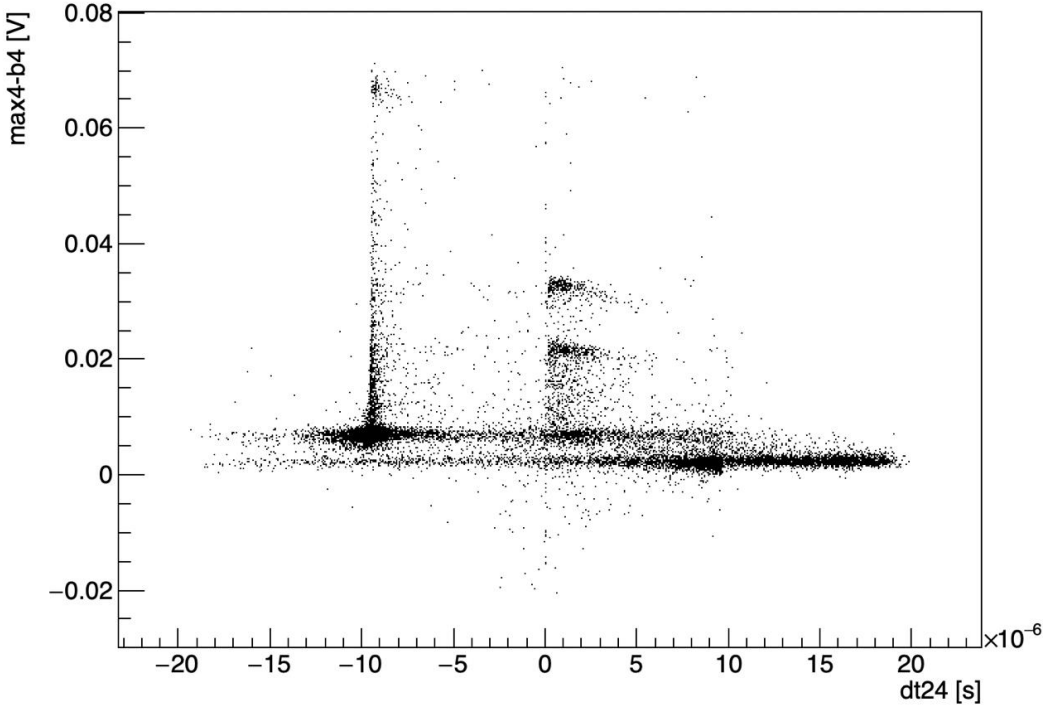


Figure 2.41: .

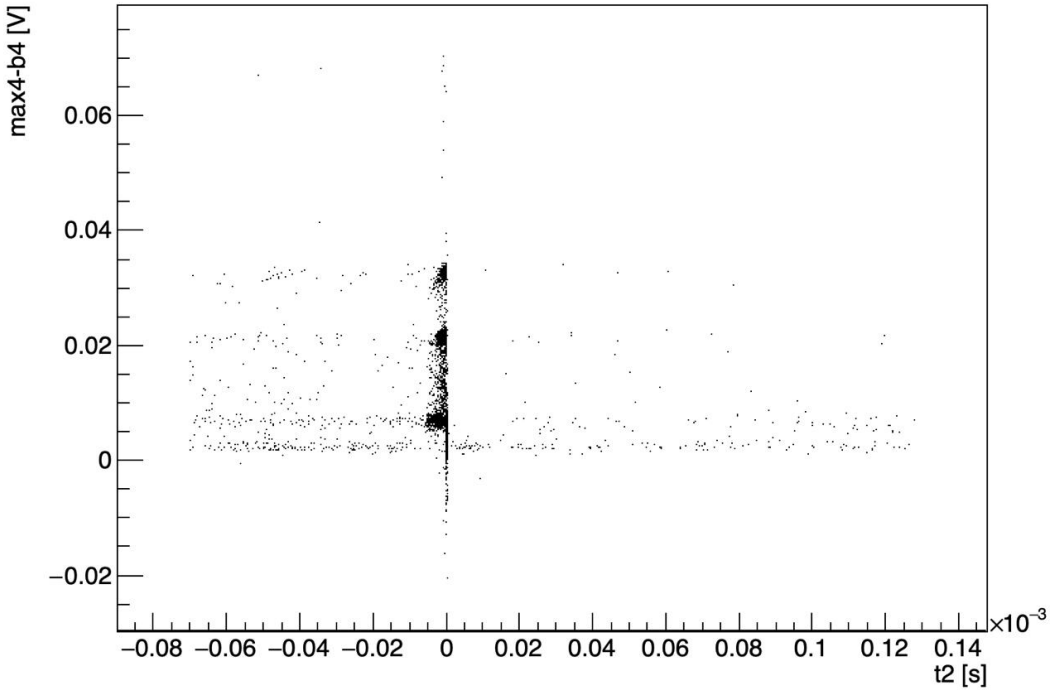


Figure 2.42: Trigger time of the LYSO for the event collected in the americium analysis.

The final check is to control the proportionality between the height of the signal and the mean value for the CZT, in order to avoid saturation and pile-up. The results before and after this cutting are presented in the Figures 2.43 and 2.44, that justify the previously

explained rejections.

The unwanted results seen in Figures 2.41 and 2.42 may belong to strange shapes of CZT signal visible in Figure 2.43, probably caused by pile-up (first linear region), electronic noise and saturation (vertical final region).

A further verification of these facts is provided by an additional analysis of the waveform, but this step is beyond the aim of the experience so it is not discussed here.

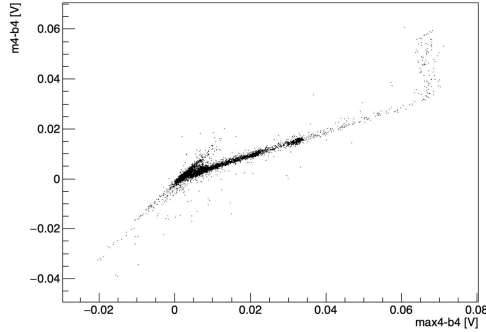


Figure 2.43: Pre cutting.

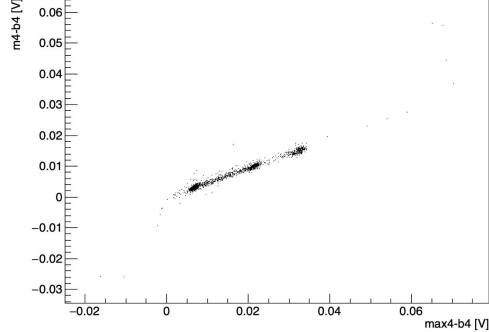


Figure 2.44: Post cutting.

### 2.4.3 Results

The usual coincidence image is reported in Figure 2.45 showing three distinguishable patterns in the CZT referring to the peaks at  $E = 202\text{keV}$  and  $E = 307\text{keV}$  of LYSO and  $E = 59\text{keV}$  from americium. The spectrum of the CZT is then reported in Figure 2.46.

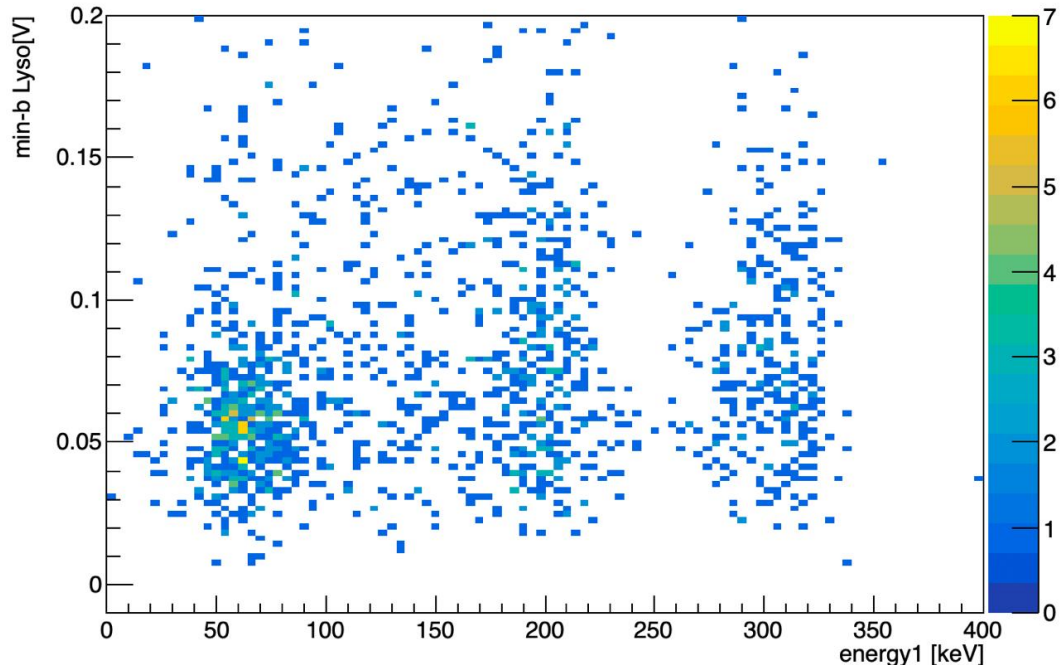


Figure 2.45: Coincidence pattern of LYSO-CZT.

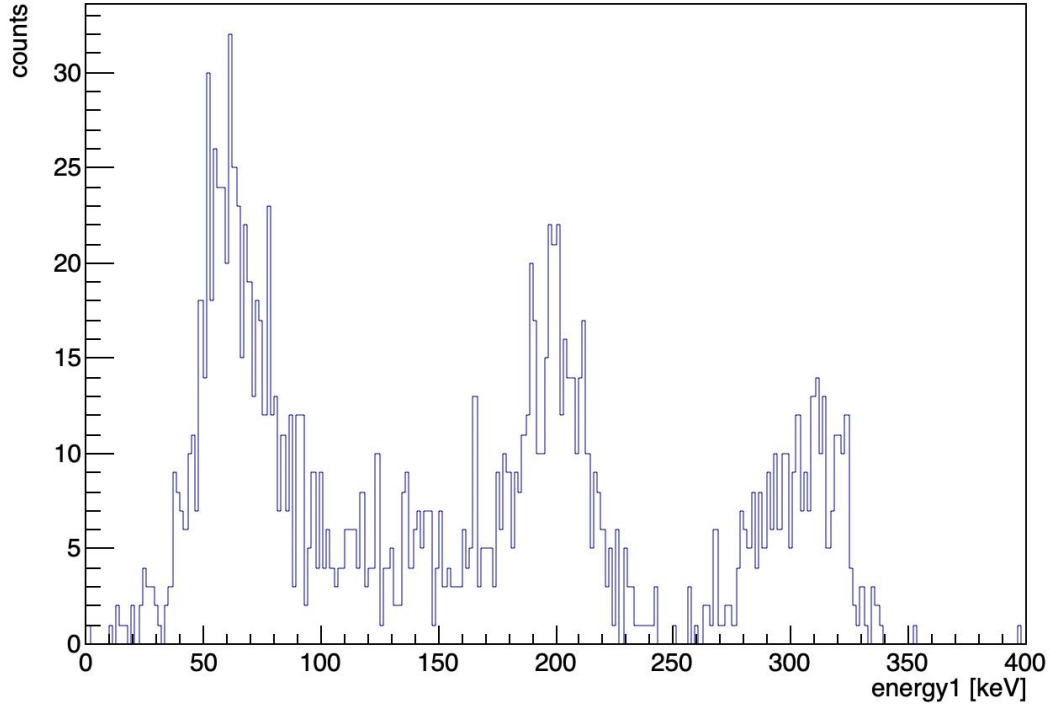


Figure 2.46: Spectrum of the CZT. Each peak is fitted with a Gaussian distribution and the energy of the peaks are reported in Table 2.2.

peak 1	$308 \pm 2$
peak 2	$200 \pm 1$
peak 3	$64 \pm 1$

Table 2.2: Mean of the Gaussian fit (with *likelihood* parameter) of the three peak in Figure 2.46.

From Table 2.2 it is clear that the LYSO peaks in the CZT are highly compatible with the expected value; however, this is not true the case of the  $E = 59\text{keV}$  peak. The reason for this discrepancy could be that the high peak at  $E = 64\text{keV}$  is indeed the sum of several Gaussian peaks, with the CZT not precise enough to resolve them. This can include the  $E = 88\text{keV}$  coming from the LYSO but at the same time, and more probably, the  $k\alpha$  ( $E = 74.969\text{keV}$  and  $E = 72.84$ ) and  $k\beta$  ( $E = 84.936\text{keV}$ ) lines of emission of the lead used to shield the apparatus. The fact that the estimation of the peaks at  $E = 59\text{keV}$  is shifted at  $E = 64\text{keV}$  is a further confirmation that the previously cited peaks have an effect: in principle we should find (and fit) 5 Gaussians. Fitting just the left side of the first peak, that should belong to the lower energy peak, the mean goes to  $(59 \pm 4)\text{keV}$  which is compatible with the americium decay expectation.

To improve this measurement, either a more resolute instrument is necessary, like a ger-

manium detector, or more statistics must be acquired, that will contribute to sharpen the peaks (the broadening of the peak depends on the Poissonian distribution of the counts). Next step is to try the identification of the alpha particle loosing energy in the LYSO. When this detector see the alpha particle, the CZT is supposed to register the photons coming from the de-excitation of the neptunium in its ground state, and *vice versa* when the CZT is hit by the LYSO's photons, the LYSO is expected to measure its  $\beta$  decay. This mechanism is visible in Figure 2.47: the coincidence measurement of LYSO and CZT is presented. Three curves are plotted: one for the CZT events in between  $E \in (280, 320)\text{keV}$  to catch the  $E = 307\text{keV}$  peak, one for the  $E = 202\text{keV}$  in the window  $E \in (180, 220)\text{keV}$ , both from the lutetium, and the last one from americium in  $E \in (40, 80)\text{keV}$  to catch the  $E = 59\text{keV}$  peak.

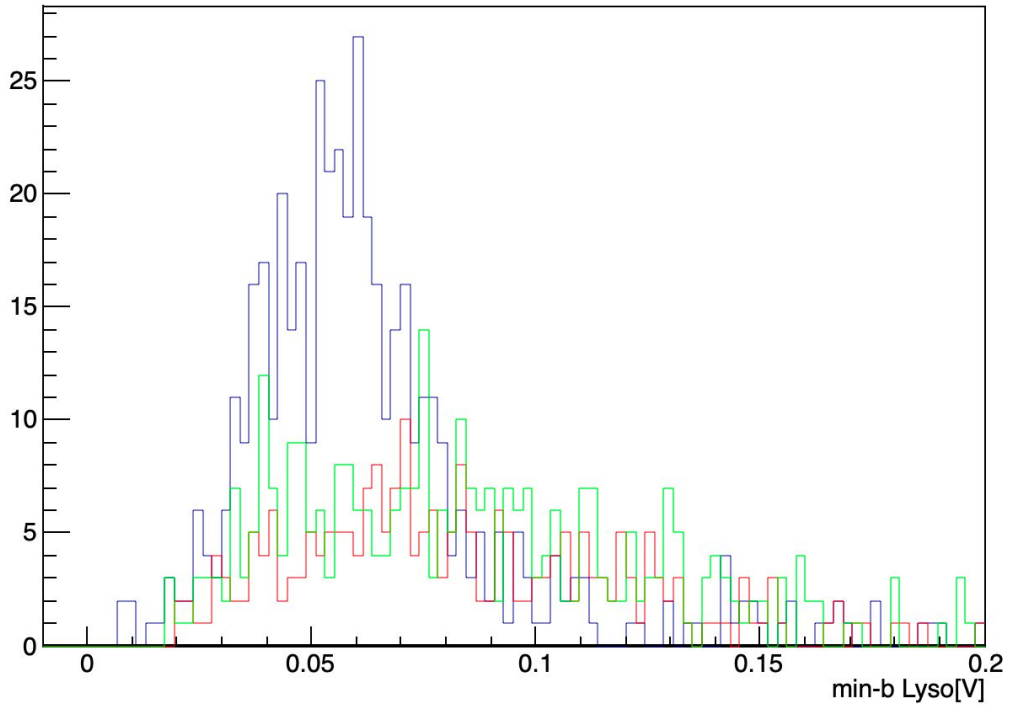


Figure 2.47: Coincidence histogram. Blue line refers to alpha particle measured by the CZT; red line refers to beta decay of lutetium (CZT measuring  $E = 307\text{keV}$ ), green line is the same beta decay of lutetium (CZT measuring  $E = 202\text{keV}$ ).

What is clear from Figure 2.47 is that the green and red line representing beta decay are overlapped, while the blue curve is different. In particular the mean value,  $\bar{m}_{blue} = 0.06$ , of this last histogram is shifted towards lower energies compared to the  $\beta$  decay,  $\bar{m}_{red} = \bar{m}_{green} = 0.08$  for both the green and red histogram. This can be identified as the fingerprint of alpha particle.

However, since alpha particles are very energetic (here they are emitted with a mean value of  $E_\alpha = 5.5\text{MeV}$ ) and they completely stops inside the LYSO, a large signal in this detector

is expected. The discrepancy with the observed data can be attributed to the effect of scintillation quenching, for which very dense ionization columns emit less light than expected, as the saturation of the detector in that zone is reached. This effect is more pronounced the greater the density of the excited molecules.

A way to distinguish between particles that promote quenching in the detector is to studying the waveform of the signal via pulse shaped discrimination.

# **Chapter 3**

## **Conclusion**

In this experience, several aspects of nuclear physics have been investigated, allowing for interesting considerations ranging from quenching to intrinsic background determination. Coincidence techniques is a powerful tool that allows to discriminate events and to do a coherent analysis of the processes going on.

After data rejection, some statistics were poor, not allowing for a sophisticated analysis. So a first improvement could be longer data taking, also introducing other known radioactive sources, to improve calibration and coincidence patter.

Americium analysis can be improved by changing the CZT with a more resolute detector and a more detailed analysis can be done, considering each waveform.